RSC Advances

PAPER

View Article Online
View Journal | View Issue

Cite this: *RSC Adv.*, 2023, **13**, 29749

Ultrasonic-induced synthesis of novel diverse arylidenes *via* Knoevenagel condensation reaction. Antitumor, QSAR, docking and DFT assessment†

Eman El-Sayed Ebead,[a] Asmaa Aboelnaga,[a] Ekhlass Nassar,[a] Mohamed M. Naguib[b] and Mahmoud F. Ismail *[c]

A series of arylidenes derivatives was synthesized under ultrasonic methodology *via* Knoevenagel condensation reaction of cyanoacetohydrazide derivative with the appropriate aldehydes and/or ketone. The anticancer properties of the newly synthesized compounds were tested against four different human cancer cell lines (HEPG-2, MCF-7, HCT-116, and PC-3); compounds **5d** and **6** demonstrated the greatest anticancer activity against all cancer cell lines. The MLR technique was used to create the QSAR model using five molecular descriptors (AATS6p, AATS7p, AATS8p, AATS0i, and SpMax4_Bhv). The examination of the constructed QSAR model equations revealed that the selected descriptors influence the tested compound's anti-proliferative activity. The descriptors identified in this work by QSAR models can be utilized to predict the anticancer activity levels of novel arylidenes derivatives. This will allow for significant cost savings in the drug development process and synthesis at pharmaceutical chemistry laboratories. According to the physicochemical properties, the results revealed that all of these compounds comply with Lipinski's Rule of Five, indicating that they may have high permeability across biological membranes and reveal drug-relevant properties. The Swiss Target Prediction webtool was used to assess the probable cellular mechanism for the promising candidate compounds (**5d** and **6**), and the results revealed that adenosine A1 receptor (ADORA1) was a common target for both compounds. ADORA1 is involved in the regulation of cell metabolism and gene transcription. ADORA1 overexpression has been linked to a variety of cancers, including colon cancer, breast cancer, leukemia, and melanoma. The docking study of tested compounds **5d** and **6** revealed that their binding scores to ADORA1 are more favorable than those of its co-crystalized ligand (DU172, selective ADORA1 antagonist) and adenosine (ADORA1 endogenous agonist), implying that they may hold great promise as an anti-cancer therapy. Density functional theory (DFT) with a (B3LYP)/6-31G (d,p) basis set was used to calculate the physicochemical parameters of these compounds. The theoretical data from the DFT computation was found to be in good agreement with the experimental values.

Received 24th August 2023
Accepted 2nd October 2023

DOI: 10.1039/d3ra05799b

rsc.li/rsc-advances

1. Introduction

In the field of heterocyclic compounds designation, there has been a markedly increased interest in the invention of new heterocyclic compounds, especially nitrogen-bearing ones, because of their prevalence in nature and also in pharmacology. Piperidine moiety is a generative basis of numerous therapeutically important compounds due to its numerous biological and pharmacological activities[1,2] including anticancer[3–5] anti-proliferative compounds against MCF-7 breast cancer and PC-3 prostate, HepG2 cancer cells,[6] antidiabetic,[7] antidepressant,[8] H_3R antagonistic,[9] antibacterial,[10] antifungal,[11,12] antiviral, anti-HIV, antineoplastic,[7] α_2c antagonists,[13] anesthetics,[14] anti-inflammatory,[15,16] hypotensive,[17] antituberculosis[18] and analgesic agent.[19] Moreover, piperidine complexes represent one of the most ubiquitous heterocyclic moieties existing in food and drug administration (FDA-approved drugs) (Fig. 1).[20]

On the other hand, cyanoacetohydrazide derivative is a particularly promising precursor in the combinatorial synthesis of functionalized heterocyclic compounds[21] because cyanoacetohydrazide possesses a variety of reactive functional groups represented in different electrophilic and nucleophilic centers.[22–26] So that, cyanoacetohydrazide is a privileged starting molecule for developing possible bioactive agents, and their derivatives represent an important class of heterocyclic

[a]*Chemistry Department, Faculty of Women for Arts, Science and Education, Ain Shams University, Heliopolis, Egypt*

[b]*Department of Biochemistry, Faculty of Science, Ain Shams University, 11566, Abbassia, Cairo, Egypt*

[c]*Department of Chemistry, Faculty of Science, Ain Shams University, 11566, Abbassia, Cairo, Egypt. E-mail: fawzy2010@sci.asu.edu.eg*

† Electronic supplementary information (ESI) available. See DOI: https://doi.org/10.1039/d3ra05799b

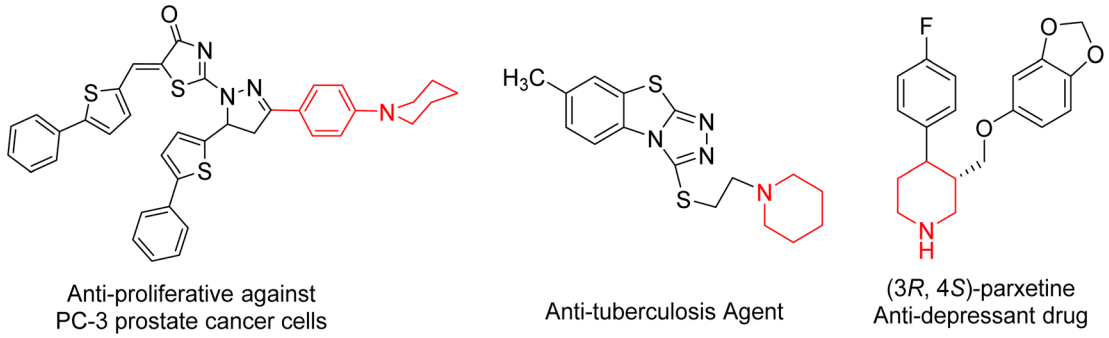

Fig. 1 Selected pharmaceutical structures containing piperidine scaffold.

compounds, they exhibited a wide spectrum of bioactivity. For example, antitumor,[27–29] anti-fungal,[30] anti-inflammatory,[31,32] anti-microbial,[33,34] as well as insecticidal[35,36] and corrosion inhibitory activities.[37]

Noteworthy, it is well known that the ultrasonic energy has become widely used in pharmaceutical and industrial applications.[38] Being a tool of green and sustainable chemistry, it is employed in organic synthesis[39] as it enhances yield and purity of products, shortens reaction time by increasing reaction rate and mass transfer, and allows using milder reaction conditions in comparison to conventional thermal methods.[40]

Accordingly, we utilized an eco-friendly method; ultrasonic waves for synthesis of 2-cyano-*N*′-(4-(piperidin-1-yl)benzylidene) acetohydrazide **3** as a synthon to synthesize novel arylidenes and heteroarylidenes. The newly synthesized compounds were confirmed *via* spectral analyses such as FT-IR, ^{1}H NMR, ^{13}C NMR, and mass spectra. These compounds were evaluated for their antitumor activity. The chemical and physicochemical properties of the biochemical arrangements can be predicted using different computational performances[41] by studying the stability of newly synthesized compounds and investigating the results of their biological evaluation by optimizing theoretical modeling with DFT/B3LYP/6-31G (d,p) density functional theory beside docking study.

2. Results and discussion

2.1. Chemistry

Initially, we documented the synthesis of 2-cyano-*N*′-(4-(piperidin-1-yl)benzylidene)acetohydrazide **3** *via* the forthright condensation of 4-(piperidin-1-yl)benzaldehyde **1** (ref. 42) with the indispensable cyanoacetohydrazide **2** (ref. 43) in absolute ethanol under both conventional[42] and ultrasonic conditions (Scheme 1). Noticeably, the ultrasonic methodology gave a better yield with higher purity in a shorter time than the conventional method, as illustrated in Scheme 1.

Structurally, compound **3** was established by using different spectroscopic data. In the IR spectrum, there are three absorption bands for C≡N, C=O and C=N functionalities at 2263, 1701, and 1610 cm^{-1}, respectively. Additionally, the ^{1}H NMR spectrum of **3** showed signals in accordance with NH, methylene, methine, piperidine and aromatic protons of the proposed structure. It was worthy of note that both ^{1}H and ^{13}C NMR spectra elucidated the presence of compound **3** in two diastereomeric isomers (*Z*-/*E*-) in the ratio 31 : 69. The chemical shift values of the signals of NH and methylene protons of the *E*-isomer showed at lower field, but the chemical shift value of the signal of the imino methine (CH=N) proton showed at higher field than the corresponding *Z*-isomer due to the coplanarity of 4-(*N*-piperidinyl)phenyl group and –NH–CO-CH_2CN moiety in the *E*-isomer, which led to extending the conjugation about it (Fig. 2).

The ratio between the two diastereomeric isomers (*Z*-/*E*-) was explicated computationally by the binding energy of both *Z*- and *E*-isomers; the *E*-isomer has a binding energy (E_T = −876.690772 a.u) smaller than the corresponding *Z*-isomer (E_T = −876.684965 a.u). Also, the energy gap of the *E*-isomer is 3.8887 eV is smaller than the energy gap of the corresponding *Z*-isomer is 4.1775 eV. It indicated that the *E*-isomer is more stable than the *Z*-one. The optimized geometry of both isomers

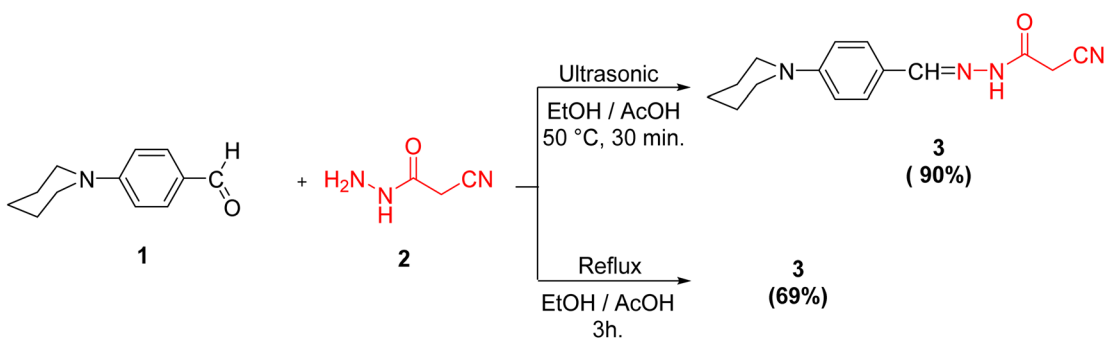

Scheme 1 Synthesis of the target compound 3.

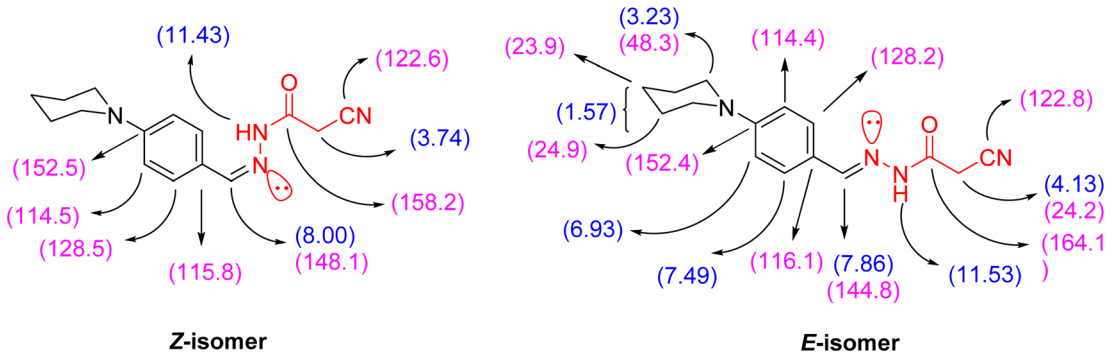

Fig. 2 ^{1}H and ^{13}C NMR values of the diastereomeric isomers of compound **3**.

clarified the coplanarity of the *E*-isomer and the letter has a dipole moment (μ = 11.696023 Debye) greater than the *Z*-isomer (μ = 8.552684 Debye) (Fig. 3).

Cyanoacetohydrazide moiety possesses manifold reaction sites, including electrophilic and nucleophilic sites. Therefore, let us dedicate our efforts to demonstrate the reactivity of the active methylene (as a nucleophilic center in the presence of a secondary base such as piperidine) of cyanoacetohydrazide derivative **3** under Knoevenagel condensation reaction using ultrasonic methodology. For example, sonication of compound **3** with a diverse range of aldehydes, like isonicotinaldehyde, 1*H*-pyrrole-2-carbaldehyde, 1*H*-indole-3-carbaldehyde and anthracene-9-carbaldehyde, beside a ketone, namely 4-chloroacetophenone, gives rise to the arylidene derivatives **4** and **5a–d**, respectively.

Interestingly, the spectral analyses of the arylidene derivatives **4** and **5a–d** unambiguously elucidated the predictable structures. For instance, the IR spectrum of **4** showed the stretching frequency of the conjugated cyano group at 2200 cm^{-1}. Indisputably, the ^{1}H NMR spectrum revealed two singlet peaks at 8.28 and 8.01 ppm compatible with HC=N and HC=C protons, and four doublet peaks: two peaks at 7.53 and 6.96 ppm with J = 8.0 Hz compatible with benzylidene protons and the other two doublet peaks at 7.91 and 7.04 ppm with J = 8.8 Hz compatible with $C_{2,6}$–$H_{(pyridine)}$ and $C_{3,5}$–$H_{(pyridine)}$ protons, respectively.

For arylidene derivative **5b**, the vanish of the cyano group from the IR which indicated the partially hydrolyzed of cyano functionality. Also, the appearance of two peaks at 189.9 and 184.9 ppm in the ^{13}C NMR spectrum indicated the presence of two carbonyl groups. Moreover, the ^{1}H NMR spectrum visibly displayed three singlet peaks at 9.93, 9.67 and 8.27 ppm corresponding to HC=N, HC=C and C_2–$H_{(indole)}$ protons, respectively. Furthermore, the mass spectrum of **5b** showed the molecular ion peak at m/z = 415.97 (36.71%) which is in

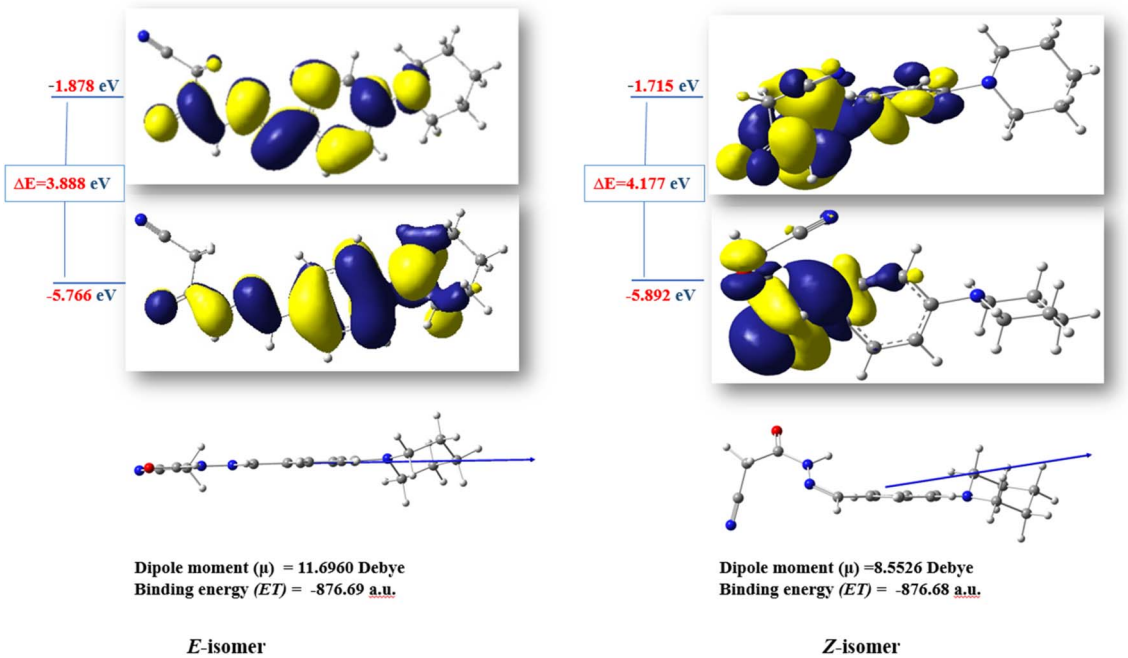

Fig. 3 The optimized structures and HOMO–LUMO energy gap of the diastereomeric isomers of compound **3**.

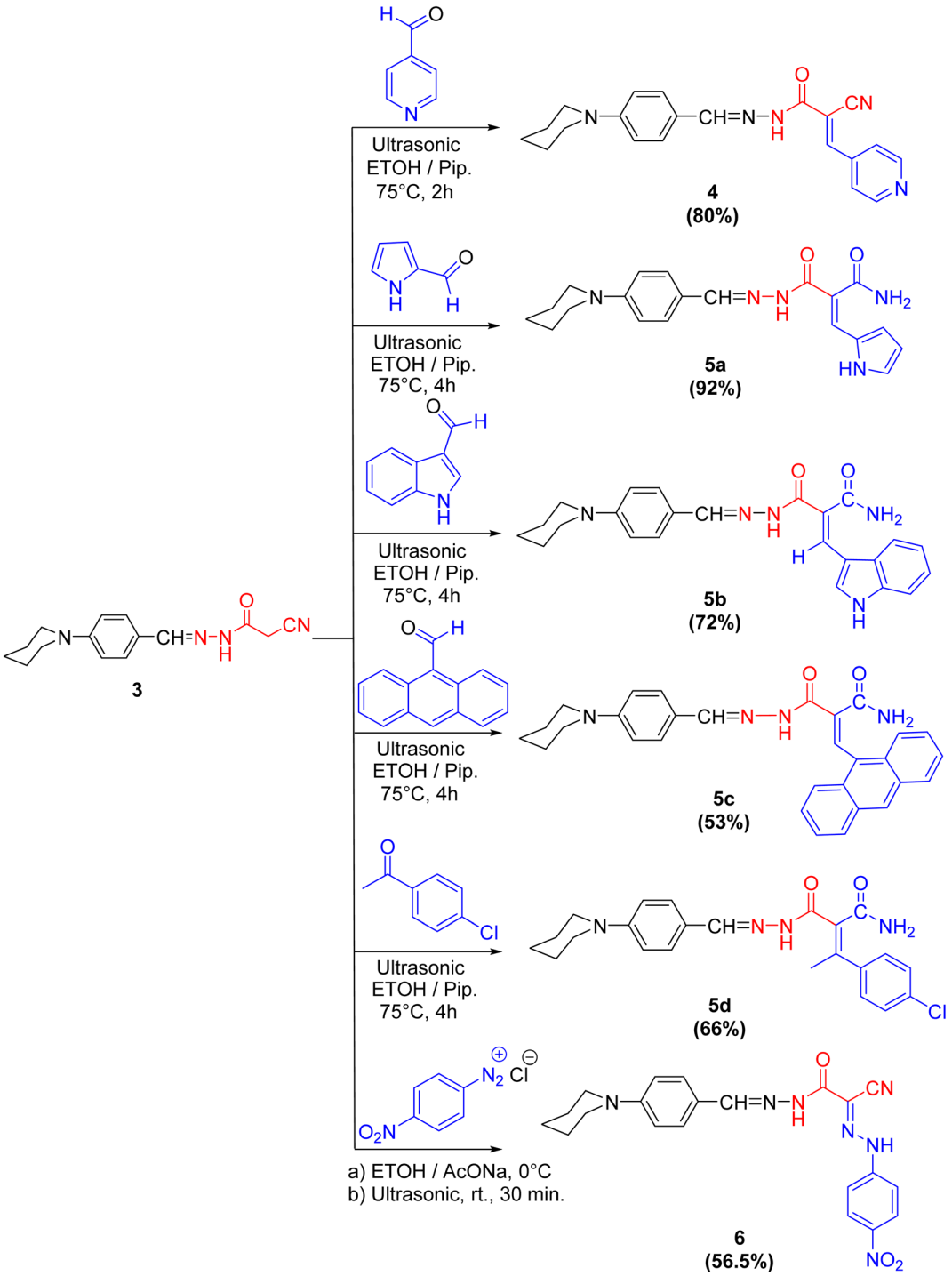

Scheme 2 Synthetic pathway to compounds **4**–**6**.

agreement with the molecular formula of the partially hydrolyzed arylidene derivative **5b** (Scheme 2).

In the coupling reaction, cyanoacetohydrazide derivative **3** was viable at the active methylene with 4-nitrobenzene diazonium chloride at ambient temperature under sonication conditions, leading to the formation of the hydrazone derivative **6** in a considerable yield. The IR spectrum displayed two bands characteristic for the asymmetric and symmetric vibrational coupling modes of the nitro group at 1515 and 1338 cm^{-1}, respectively. Further, in ^1H NMR spectrum of compound **6**, two broad singlet peaks commutable with D_2O at 9.66 and 6.58 ppm compatible with two NH protons were displayed.

It was notably that, in case of formation of compounds **5a–d**, the nitrile group is partially hydrolyzed to the corresponding amide but through formation compounds **4** and **6**, the nitrile group is preserved, because of isonicotinaldehyde is very reactive aldehyde due to pyridine ring act as an electron withdrawing group especially in position 2- and 4-, which accelerate the

Table 1 Cytotoxicity (IC_{50}) of tested compounds on different cell lines[ac]

Compound no.	*In vitro* cytotoxicity IC_{50}[b] (μM)			
	HePG2	HCT-116	MCF-7	PC3
DOX	4.50 ± 0.2	5.23 ± 0.3	4.17 ± 0.2	8.87 ± 0.6
3	39.72 ± 3.5	25.34 ± 3.8	24.07 ± 3.6	38.60 ± 4.3
4	29.64 ± 3.0	23.79 ± 3.5	20.35 ± 2.5	31.38 ± 3.8
5a	24.31 ± 2.6	14.11 ± 2.4	21.07 ± 2.3	34.76 ± 2.9
5b	12.89 ± 0.9	17.70 ± 1.4	17.22 ± 0.6	14.65 ± 1.8
5c	31.83 ± 2.1	44.06 ± 3.2	45.20 ± 2.0	41.34 ± 3.6
5d	6.94 ± 0.4	11.62 ± 1.0	5.60 ± 0.4	10.51 ± 1.3
6	10.11 ± 3.1	8.23 ± 3.3	7.61 ± 3.4	13.83 ± 3.8

[a] The data are expressed as the mean of three replicates ± standard deviation. [b] IC_{50} (μM): 1–10 (very strong). 11–20 (strong). 21–50 (moderate). 51–100 (weak) and above 100 (non-cytotoxic). [c] DOX: doxorubicin.

formation of compound **4** in a time not enough to hydrolyze the nitrile group. Also, the formation of compound **6** was done at ambient temperature and that was not enough to hydrolyze it.

2.2. Pharmacology

2.2.1. Cytotoxicity and antitumor evaluation. *In vitro* cytotoxicity of the newly synthesized compounds **3–6** against four different human cancer cell lines (HEPG-2, MCF-7, HCT-116, and PC-3) was investigated. Cytotoxicity is measured in terms of IC_{50} (the concentration at which half-maximal inhibition is recorded). For comparison, doxorubicin (Dox) was utilized as a standard anticancer drug.[44]

According to our initial screening results, compounds **5d** and **6** had the highest cytotoxic activity, while compounds **3**, **4**, **5a**, and **5b** showed intermediate cytotoxic activity. The cytotoxicity of compound **5c** was minimal (Table 1).

2.3. Structure activity relationship's (SAR's)

The structural activity relationships (SAR) were studied by comparing the experimental cytotoxicity of the newly synthesized compounds according to their structures as follows:

(1) The structure of the parent compound **3** is based on the presence of the piperidine moiety, which is an important core of many drug molecules with antihistamine, anticancer, and antibacterial properties[45] and hydrazone moiety, which is important for bioactivity as it undergoes azo reduction into toxic amine derivatives. In addition, the hydrazone functionality is known for its anticancer properties.[46,47]

(2) The cytotoxic activity of the parent compound **3** was found to be in a moderate value compared to the standard drug, doxorubicin which could be due to the presence of piperidine and hydrazone moieties.

(3) Different moieties possessing different lipophilic heteroaryl and phenyl rings with a variety of electron withdrawing and electron donating groups were added to the parent compound **3** in order to investigate their anticancer activities.

(4) Introduction of nitrogen bearing heterocyclic ring systems as pyridine, pyrrole and indole rings in compounds **4**, **5a** and **5b**, respectively, improve the cytotoxic activity towards all

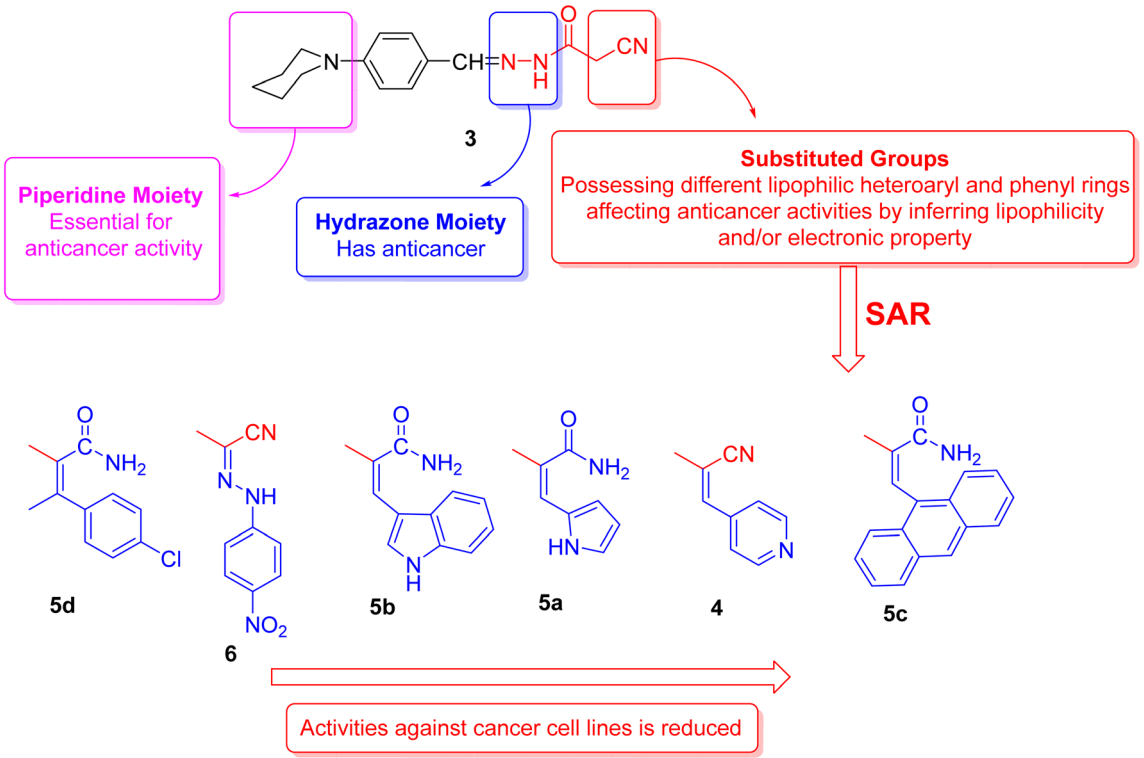

Fig. 4 Structure activity relationship of piperidine derivatives.

Table 2 Studied compounds and their observed pIC_{50}

Compound no.	IC_{50} (μM)	pIC_{50} (M)
3	24.07	4.6185
4	20.35	4.6914
5a	14.11	4.8505
5b	12.89	4.8897
5c	31.83	4.491
5d	5.6	5.2518
6	7.61	5.1186

cell lines as compared to compound **3** because the nitrogen bearing heterocycles and their products show several essential features and are being utilized in different ways as anticancer.

(5) Compounds **5d** and **6** showed the highest anticancer activity towards all cell lines, this could be due to:

(a) The presence of hydrophobic chlorobenzene moiety (compound **5d**) that may be essential for binding with the active site of many cellular enzymes, and electron donating group (Cl) that promotes the antitumor effect.[48]

(b) The presence of extra hydrazone moiety and nitro group (compound **6**) that may be critical for anticancer activity.

(6) Incorporation of anthracene nucleus (compound **5c**) showed lowest anticancer activity towards all cell lines as compared to the other tested compounds.

(7) Regarding the SAR of tested compounds (Fig. 4), there was a consistent relation between the lipophilicity and/or electronic property of the substituent groups and the antiproliferative activity. The introduction of a more nucleophilic and a lipophilic substituent to the parent compound **3** enhances the potency against cancer cell lines.

3. Quantitative structure–activity relationships (QSAR)

Quantitative structure–activity relationships (QSAR) are effective tools for drug discovery.[49,50] We calculated multidimensional molecular descriptors (constitutional, topological, physicochemical, geometrical, and quantum) to find molecular descriptors associated to the anti-proliferative activity of the investigated compounds. We use statistical approaches to build QSAR models to achieve this goal.[51] In this study, we employed the tested compounds to build QSAR models. Multiple linear regression (MLR) is the most widely used method in the development of QSAR due to its simplicity and robustness.[52] Internal and external validations are used to test the predictive capacity of the produced models.

3.1. The studied compounds

To develop the QSAR molecular modeling, we used the experimental IC_{50} values of the tested compounds that showed strong and moderate anti-cancer activities ($IC_{50} < 35$). In QSAR modeling, we don't use the activity in the form of IC_{50} (μM) but rather we need to convert it to the log scale to get pIC_{50} level (M) and this was done through the following equation ($pIC_{50} = -\log_{10}(IC_{50} \times 10^{-6})$), which are presented in Table 2.

3.2. Calculation of molecular descriptors

The studied molecules were initially subjected to energy minimization and then saved as SD files for later use in descriptor calculation. The calculation of molecular descriptors for the studied molecules began with the import of the various molecules in SD file format into the PaDEL-Descriptor software, which creates 1875 descriptors (1444 1D, 2D, and 431 3D descriptors).[53] Data pretreatment was performed to eliminate uninformative descriptors from the generated descriptors pool (low variance descriptors, zeros and NA descriptors).

3.3. Statistical methods

To construct QSAR model for the seven tested molecules obtained by *in vitro* synthesis, we used the statistical methods presented below.

Table 3 Selected descriptors used in the QSAR model[a]

Descriptors	Description	Class	MLR of the selected descriptors
AATS6p	Average Broto–Moreau autocorrelation – lag 6/weighted by polarizabilities	2D	RSE: 0.02785
AATS7p	Average Broto–Moreau autocorrelation – lag 7/weighted by polarizabilities	2D	Multiple *R*-squared: 0.9982
AATS8p	Average Broto–Moreau autocorrelation – lag 8/weighted by polarizabilities	2D	Adjusted *R*-squared: 0.9894
AATS0i	Average Broto–Moreau autocorrelation – lag 0/weighted by first ionization potential	2D	*F*-Statistic: 112.8
SpMax4_Bhv	Largest absolute eigenvalue of Burden modified matrix – *n* 4/ weighted by relative van der Waals volumes	2D	*p*-Value: 0.07135

[a] MLR: multiple linear regression; RSE: residual standard error.

3.3.1. Selection of the best descriptors for QSAR modeling. To get the best fit for a multiple regression model, it is important to include the most significant subset of predictors from the dataset. The *regsubsets* function of the *Leaps* R-based regression subset selection package[54] was used to performs an exhaustive search to identify the different molecular descriptors that will contribute to the development of the best QSAR model. The best descriptors were selected by evaluating the combination of the main parameters used in this approach that are correlation coefficient (R^2) (eqn (1)), adjusted correlation coefficient ($R_{adj}{}^2$) (eqn (2)), the mean squared error (MSE) (eqn (3)) that leads to the best MLR model. Five different molecular descriptors of the studied compounds that belong to different classes (1D, 2D) were selected to develop MLR models Table 3. The model was then evaluated using the best predictors that generated an acceptable model of adjusted R^2: 0.9894 ($R^2 > 0.6$), high *F*-statistic: 112.8 ($F > 0.33$) and the level of significant (*p*-value): 0.07135 indicates that the model equation is statistically significant with level greater than 90%.[55]

$$R^2 = 1 - \frac{\sum_{i=1}^{n} (Y_{obs} - Y_{calc})^2}{\sum_{i=1}^{n} \left(Y_{obs} - \overline{Y}_{calc}\right)^2} \quad (1)$$

$$R_{adj}{}^2 = \frac{(n-1) \times R^2 - P}{n - 1 - P} \quad (2)$$

$$MSE = \frac{1}{n} \sum_{i=1}^{n} (Y_{obs} - Y_{calc})^2 \quad (3)$$

where Y_{obs} is the value of the observed response, Y_{calc} is the value of the predicted response, Y_{calc} is the average value of observed/predicted responses, p is the number of explicative variables in the model, and n is the number of individuals.

3.3.2. Analysis of the structure–activity relationship. After calculating these descriptors for the investigated molecules Table 4, we identify the quantitative association between these descriptors and the anti-proliferative activity of the tested compounds (pIC_{50} level). The quantitative relationship was built using the ChemMaster1.1 software and the MLR statistical approach for expressing QSAR models.

The ChemMaster1.1 software (**https://crescentsilico.wordpress.com/chemmaster/**) was used for the model building based on MLR approach that establishes the relationship between the dependent variable (pIC_{50}) and the independent variables (molecular descriptors)[56] according to the following equation (eqn (4)).[57]

$$Y = k_1x_1 + k_2x_2 + k_3x_3 + \ldots C \quad (4)$$

where '*k*'s and '*x*'s are, respectively, regression coefficients and independent variables, Y is the dependent variable, and 'C' represents intercept or regression constant.

After identifying the most significant molecular descriptors, we divided the database into two sets (training and test). Thus, the training and test sets include 75% and 25% of the total data, respectively.[58] The training set was used to create QSAR models, whereas the test set was used to assess the effectiveness of the developed model. The Kennard Stone method,[59] which is supplied by the ChemMaster1.1 software, was used to divide the data set into training and test sets.

3.3.3. Statistical testing and validation of the QSAR model. Following the completion of the model construction, the built models were subjected to internal and external validation assessments Some parameters from the ChemMaster1.1 program, such as correlation coefficient (R^2), adjusted correlation coefficient ($R_{adj}{}^2$), and cross-validation coefficient ($R_{cv}{}^2$) (eqn (5)) are relevant for internal validation Table 5.

$$R_{cv}{}^2 = 1 - \frac{\sum (Y_{obs}(train) - Y_{calc}(train))^2}{\sum \left(Y_{obs}(train) - \overline{Y}_{calc}(train)\right)^2} \quad (5)$$

where Y_{obs} (train) is the value of the observed response, Y_{calc} (train) is the value of the response predicted by leave-one-out cross-validation (Loo-cv), Y_{calc} (train) is the mean value of the observed/predicted responses.

The R^2 defines the goodness of fit of the QSAR model. A QSAR model is considered acceptable when it has an R^2 value > 0.6 for the training set. This model has an R^2 of 0.99 for the training set. The value of $R_{cv}{}^2$ should be more than 0.5 that indicates the accuracy of the obtained QSAR model through MLR technique.[60] The value of $R_{cv}{}^2$ less than R^2 value indicates the fragility and weakness of the model when excluding any element of the training set. Therefore, it is apparent that the five descriptors in eqn (6) show a strong linear correlation with the biological activity of pIC_{50}.

$$pIC_{50} = +0.1495 \times AATS6P + 0.04 \times AATS7P - 0.0882 \times AATS8P + 0.0162 \times SPMAX4\_Bhv + 0.1048 \times AATS0i + 4.7819 \quad (6)$$

An external validation assessment was performed to determine the developed model's ability to predict the activities of the external test set compounds. Compounds from the series of

Table 4 Calculated descriptors values

Compound no.	AATS6p	AATS7p	AATS8p	AATS0i	SpMax4_Bhv
3	1.3495	1.3192	1.4282	160.1803	3.4539
4	1.2542	1.2236	1.3132	162.531	3.4523
5a	1.3177	1.2991	1.2796	160.643	3.5643
5b	1.3895	1.3419	1.2944	157.6286	3.5792
5c	1.229	1.3354	1.3717	160.462	3.5364
5d	1.4044	1.3469	1.309	163.3607	3.5039
6	1.3196	1.2695	1.2569	165.019	3.4937

Table 5 The validation parameters of the QSAR model[a]

	R^2	RMSE	MSE	$R_{cv}{}^2$
Training set	0.99	0	0	0.6
Test set	0.52	0.091	0.092	

[a] RMSE: the root mean square error.

Table 6 The observed and predicted values of anticancer biological activities by the QSAR models developed based on the training set and testing set

Compound no.	pIC_{50}	Pred. pIC_{50}
3	4.6185	4.62
4	4.6914	4.7
5a	4.8505	4.84
5b	4.8897	4.79
5c	4.491	4.5
5d	5.2518	5.3
6	5.1186	5.21

molecules investigated in this work are included in the test set, but they did not contribute to the construction of the QSAR models.

The external ability of the QSAR models to predict the activity of the test set molecules was assessed by calculating the correlation coefficient R^2 test between the observed pIC_{50} values and the predicted pIC_{50} values after the inclusion of the test set[61] (Table 6).

The model is statistically acceptable in prediction when the value of R^2 test is greater than 0.5 and can be applied to new external data.[62] This model has an R^2 of 0.52 for the test set. As a result, external validation of the QSAR models ensures that these models have a high predictive potential for pIC_{50} values.

Fig. 5 illustrates the correlation between the observed and expected activity values of pIC_{50}. The latter are derived for the molecules in both the test and training sets using a QSAR model based on the MLR approach. Fig. 5 shows that the distribution of observed and predicted pIC_{50} values is significantly correlated, which is attributable to the low MSE value achieved. As a result, it is obvious that the experimentally measured values and the QSAR model predictions are correlated.

4. Physicochemical properties

A successful drug candidate should achieve a precisely balanced combination of physicochemical properties and pharmacokinetics. ADMETlab 2.0, which is implemented as a publicly accessible web server with an easy-to-use interface, was used to calculate the overall physicochemical properties of the test compounds (Table 7).

To have robust membrane permeability, a drug candidate must have a molecular weight ≤ 500, partition coefficient values in the octanol/water system ($\log P$) ≤ 5, and a number of hydrogen bond donors and acceptors ≤ 5 and ≤ 10, respectively.[63] All of the compounds studied had hydrogen bond acceptors (n_{HA}) of less than 8 and hydrogen bond donors (n_{HD}) of less than 5. This is consistent with Lipinski's rule of five, indicating that these chemicals may have strong permeability or absorption properties across biological membranes. Furthermore, the majority of the compounds' lipophilicity, expressed as $\log P$, was found to be less than 5, confirming their drug-relevant properties.

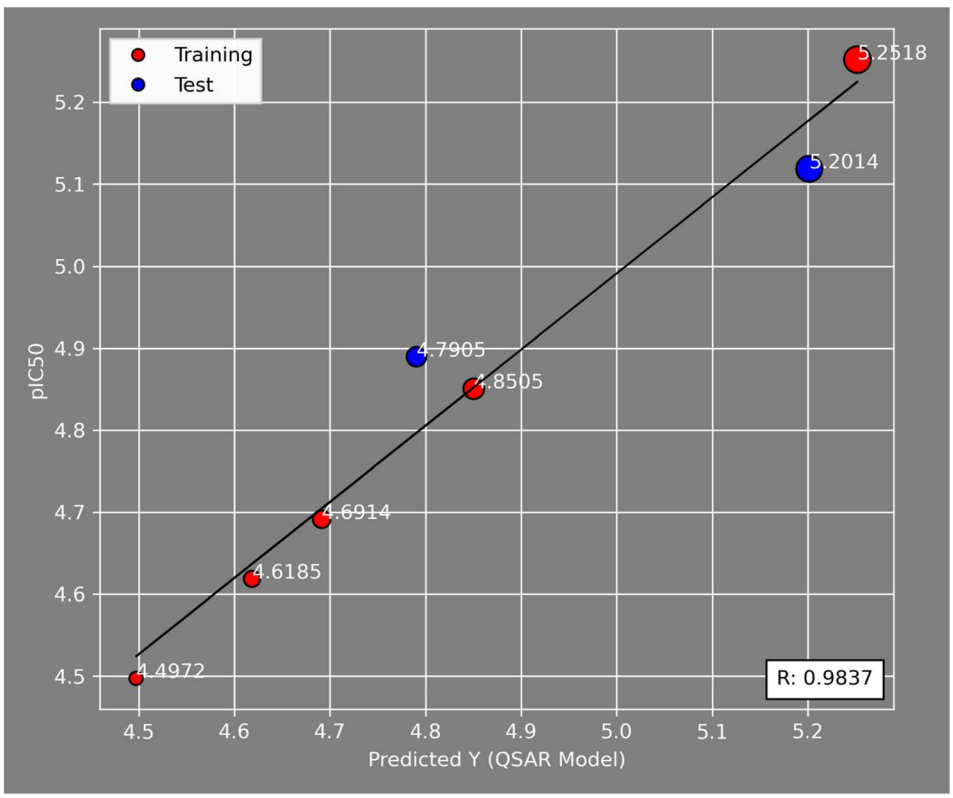

Fig. 5 Correlations between the observed activity (pIC_{50}) values and the predicted ones *via* the MLR model.

Table 7 Calculated physicochemical properties[a]

Compound no.	MW	n_{HD}	n_{HA}	Log *P*	Lipinski's rule	Log *S*	QED
3	270.15	1	5	2.581	Accepted	−4.048	0.672
4	359.17	1	6	3.551	Accepted	−4.453	0.358
5a	365.19	4	7	2.807	Accepted	−4.213	0.24
5b	415.2	4	7	3.715	Accepted	−4.814	0.189
5c	476.22	3	6	5.432	Accepted	−6.462	0.102
5d	424.17	3	6	4.451	Accepted	−5.031	0.243
6	419.17	2	10	4.926	Accepted	−6.068	0.402

[a] Where; MW, molecular weight; n_{HA}, number of hydrogen bond acceptor; n_{HD}, number of hydrogen bond donor; log *S*, logarithm of aqueous solubility value, log *P*, logarithm of the *n*-octanol/water distribution coefficient; QED, a measure of drug-likeness based on the concept of desirability.

QED is a drug-likeness metric built on the concept of desirability. QED is determined by integrating the results of desirability functions based on eight drug-likeness-related variables, including MW, log P, n_{HA}, n_{HD}, the number of aromatic rings (n_{Ar}), and the number of alerts for undesirable functional groups. The average QED for attractive compounds is 0.67, 0.49 for unfavourable compounds, and 0.34 for unattractive compounds regarded as too complex.[64] Compound **3** may have drug-like properties.

5. Molecular docking studies

Focused highlights and molecular docking studies are to be conducted for the most promising candidate compounds (compounds **5d** and **6** that showed the highest cytotoxic activities towards the cancer cell lines) in this study to reveal the probable mechanism for their anticancer potency. The probable molecular targets for these compounds were investigated using SwissTargetPrediction (**http://www.swisstargetprediction.ch/index.php**) webtool provided by Swiss Institute of Bioinformatics (**https://www.sib.swiss/**) that allows the identification of the most probable macromolecular targets of a small molecule based on a combination of 2D and 3D similarity with a library of 370 000 known actives on more than 3000 proteins from three different species (*Homo sapiens*, *Mus musculus* and *Rattus norvegicus*).[65]

The results of the target prediction revealed the presence of many targets for each compound from various categories including, G-protein coupled receptors (GPCRs), ion channels, kinases, and nuclear proteins. Adenosine A1 receptor (ADORA1; UniProt id: p30542) was found to be the common target for both compounds **5d** and **6** (Table 8).

The adenosine A1 receptor is one member of the adenosine receptor group of G protein-coupled receptors with a high affinity for adenosine, which serves as its endogenous ligand.[66] ADORA1 is known to block adenylate cyclase, lowering the level of cyclic adenosine monophosphate (cAMP) and regulating cell metabolism and gene transcription.[67] ADORA1 has been found to be overexpressed in a variety of cancers, including colon cancer,[68] breast cancer,[69] leukemia,[70] and melanoma.[71]

Table 8 The probable molecular targets for compounds **5d** and **6**

Compound no.	The probable molecular targets
5d	PIK3CB (PI3-kinase p110-beta subunit)
	PIK3CA (PI3-kinase p110-alpha subunit)
	F9 (coagulation factor IX)
	PPID (peptidyl-prolyl *cis–trans* isomerase D)
	MAOB (monoamine oxidase B)
	GSK3B (glycogen synthase kinase-3 beta)
	CHRM4 (muscarinic acetylcholine receptor M4)
	ITK (tyrosine-protein kinase ITK/TSK)
	MMP13 (matrix metalloproteinase 13)
	ADORA1 (adenosine A1 receptor)[a]
	ADORA3 (adenosine A3 receptor)
	ABL1 (tyrosine-protein kinase ABL)
	GABRA2 (GABA receptor alpha-2 subunit)
	STK17B (serine/threonine-protein kinase 17B)
	STK17A (serine/threonine-protein kinase 17A)
6	EDNRA/B (endothelin receptor ET-A/B)
	SCN9A (sodium channel protein type IX alpha subunit)
	TBXA2R (thromboxane A2 receptor)
	EPHX1 (epoxide hydrolase 1)
	AURKA/B (serine/threonine-protein kinase Aurora-A/B)
	MAPK8 (c-Jun N-terminal kinase 1)
	MAPK10 (c-Jun N-terminal kinase 3)
	JAK1/2 (tyrosine-protein kinase JAK1/2)
	PTGS2 (cyclooxygenase-2)
	ESR2 (estrogen receptor beta)
	IMPDH2 (inosine-5′-monophosphate dehydrogenase 2)
	ADORA1 (adenosine A1 receptor)[a]

[a] The common probable molecular target for compounds **5d** and **6.**

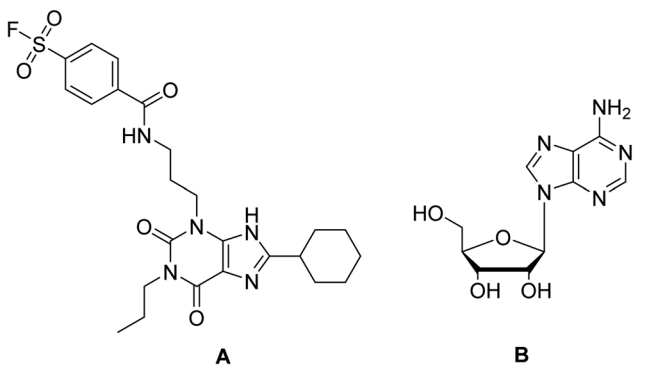

Fig. 6 Reference compounds used in molecular docking (A) DU172, selective A1 receptor antagonist. (B) Adenosine, A1 receptor endogenous agonist.

Table 9 The docking binding free energies (ΔG) and residues of interaction

Compounds	ΔG (kcal mol^{-1})	Interacted ligand binding pocket residues
5d	−9.834	Val62, Leu65, Ala66, Ile69, Val83, Val87, Leu88, Cys169, Phe171, Glu172, Met180, Leu250
6	−9.17	Tyr12, Asn70, Phe171, Glu172, Leu250, Tyr271, Ile274
Adenosine (endogenous agonist)	−6.578	Ala66, Ile69, Val83, Val87, Cys169
DU172 (co-crystalized ligand & receptor antagonist)	−8.763	Ala66, Phe171, Glu172, Leu250, Leu253, Ile274, His278

ADORA1 has been found to be upregulated in hepatocellular carcinoma (HCC) tissues, where it functions as an oncoprotein and a promoter of cell proliferation *via* the PI3K/AKT signaling pathway.[72] ADORA1 has been found to be overexpressed in a variety of breast cancer cell lines,[69] where it affects the transcriptional activity of the estrogen receptor-α (Erα) in breast cancer cells.[73]

In the present study, docking of the synthesized compounds **5d** and **6** and co-crystalized reference ligands, DU172 (4-(3-(8-cyclohexyl-2,6-dioxo-1-propyl-1,2,6,7-tetrahydro-3*H*-purin-3-yl) propyl)carbamoyl)benzenesulfonyl fluoride; one of the selective antagonist of ADORA1 and receptor endogenous agonist adenosine (Fig. 6) with ADORA1 (PDB: 5uen) were performed using AutoDock vina modeling simulation software, by placing the small molecules into the extracellular ligand binding pocket of the target in order to preliminarily predict the protein-binding affinity, as well as the preferred orientation of the docking pose. The docking results, presented as binding free energy and the interacting ligand binding pocket residues, are tabulated in (Table 9).

The proposed binding mode of co-crystalized ligand, DU172 and endogenous agonist, adenosine showed an affinity value of

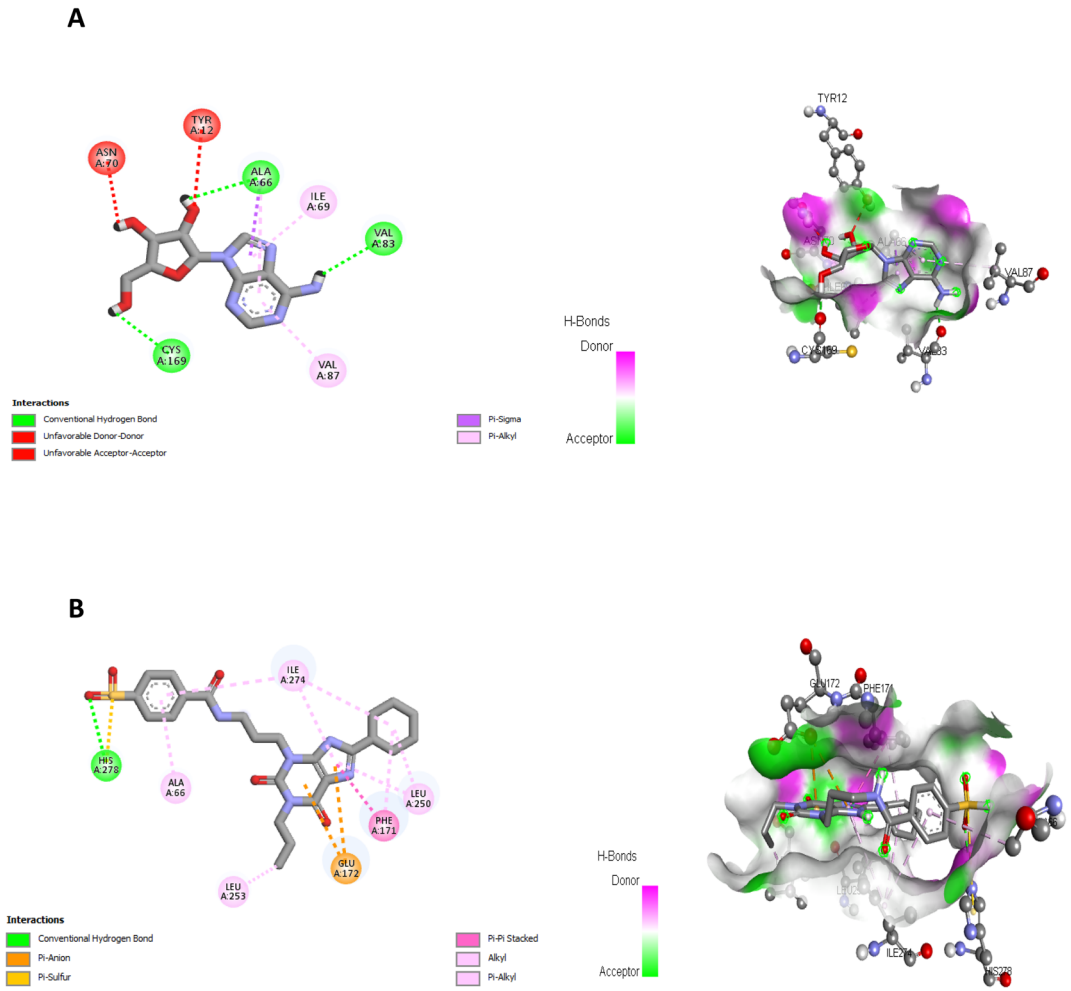

Fig. 7 (A) Interactions of ligand binding pocket residues with adenosine (3D (right) and 2D (left)). (B) Interactions of ligand binding pocket residues with DU172 (3D (right) and 2D (left)).

−8.763 and −6.578 kcal mol^{-1}, respectively while the studied compounds **5d** and **6** showed binding energies −9.834 and −9.17 kcal mol^{-1}, respectively (Table 9).

Comparing to the binding mode of DU172 and adenosine (Fig. 7), we found that the compound **5d** form extensive hydrophobic interactions with non-polar amino acid residues that form the binding pocket due to the presence of hydrophobic chlorobenzene moiety and electron donating group (Cl), therefore it binds more strongly to the target as compared to that of the co-crystalized ligand (Fig. 8). The presence of nitrobenzene moiety in compound **6** favors the formation of a number of nonpolar and hydrogen bonds with the amino acid side chains in the binding pockets, making the binding energy is more favorable than that in case of the co-crystalized ligand (Fig. 9).

Finally, the binding affinities correlates with the cytotoxicity activity of the tested compounds suggesting that the anticancer activities of the tested compounds may be related to their ability to antagonize and block the action of the extracellular adenosine on ADORA1 receptor signaling in cancer cells, leading to cell death.

6. Theoretical investigation

6.1. Optimization geometry

Density functional theory at the (B3LYP)/6-31G (d,p) level, was used for theoretical analysis of the energies and the geometry of both **3** *Z*- and *E*-isomers and its derivatives **4**, **5a–d** and **6** (Fig. 1 and 10).

By studying the optimum geometry of the investigated compounds, it found that the presence of planner benzene ring attached to the piperidine ring which acquires a slightly warped chair shape and the cyanoacetohydrazide moiety making these compounds non planner.[74] This non-planarity is a key factor in both its activity and biological activity, as all investigated compounds showed high and moderate antitumor activity, especially compounds **5b**, **5d**, and **6**.

The presence of indole, 4-chlorophenyl, and 4-nitrophenyl rings in **5b**, **5d**, and **6** respectively, provides structural diversity and electronic effects in these compounds since these rings have distinct electronic properties; for example, the non-planarity of the indole pyrrole ring can affect their interactions with biomolecules. Also, the withdrawal groups, 4-

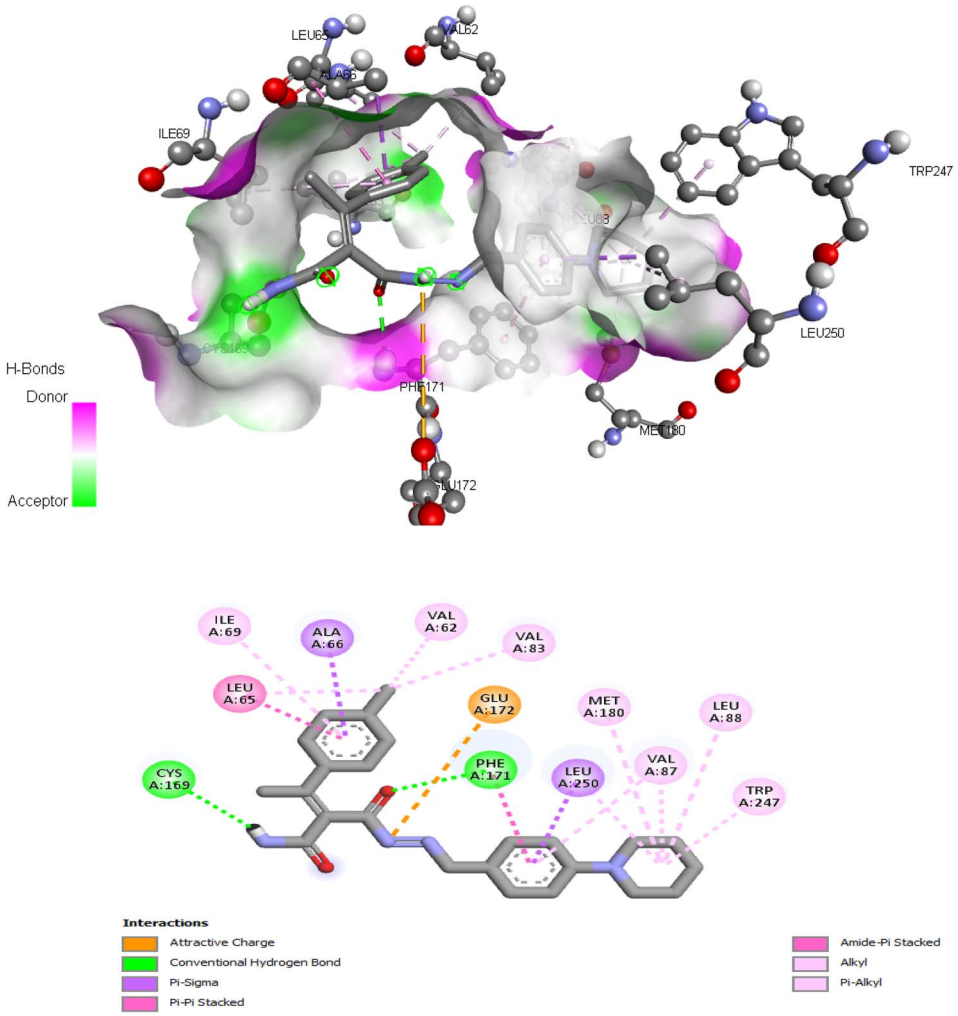

Fig. 8 Interactions of ligand binding pocket residues with compound **5d** (3D (up) and 2D (down)).

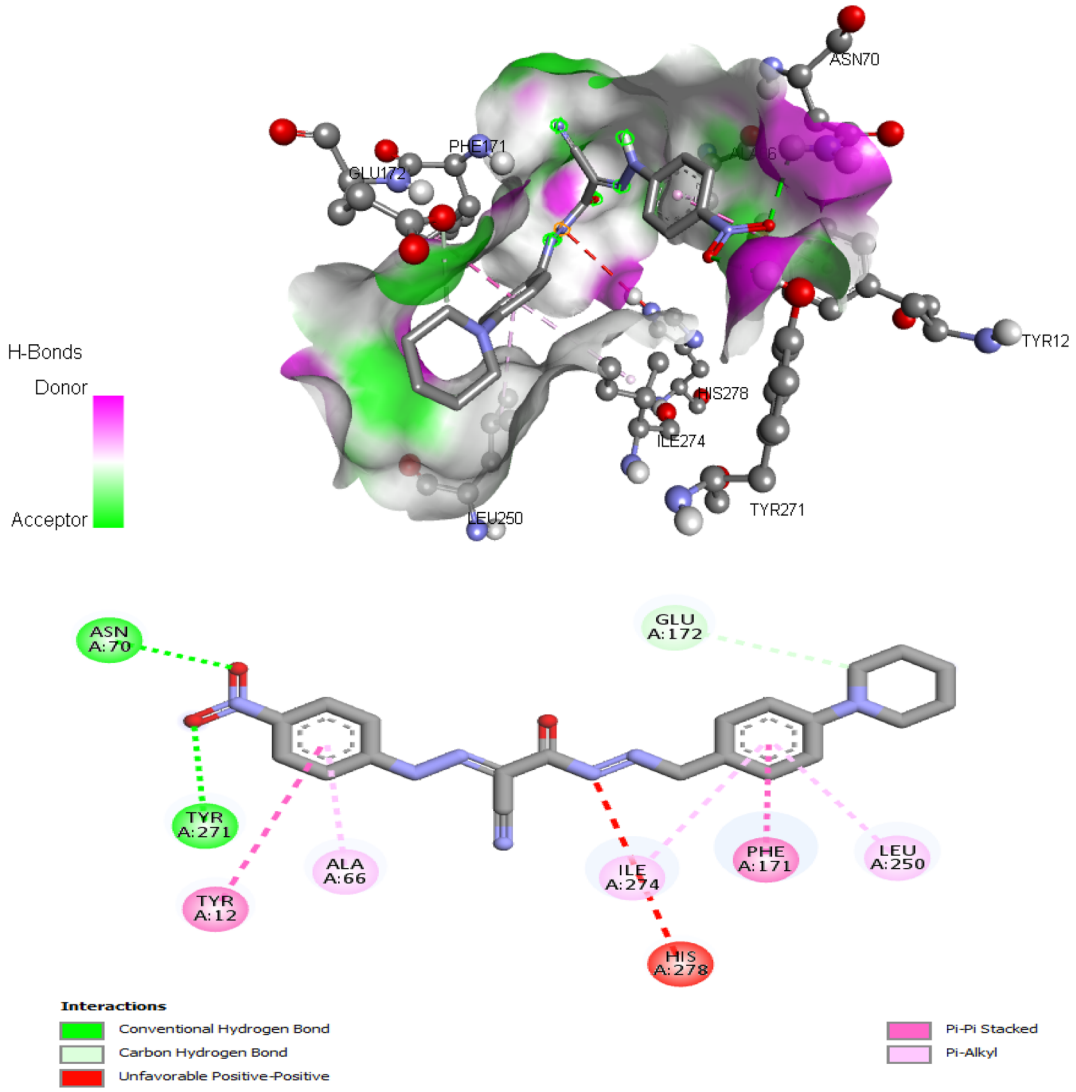

Fig. 9 Interactions of ligand binding pocket residues with compound **6** (3D (up) and 2D (down)).

chlorophenyl and 4-nitrophenyl, positively affect the biological activities of the investigated compounds.[75]

The dipole moment values of the investigated compounds were analyzed from the DFT results, the values of the dipole moment were between 6.2518-11.6960 Debye. The dipole moments tell us about the charge separation in a molecule. The lower the difference in electronegativity of bonded atoms, the lower the dipole moment. Compound **5a** demonstrated the lowest value dipole moment of 6.2518 Debye due to the presence of pyrrole rings that cause the generation of weak dipole moment.[76]

Moreover, the polarizability increases as the volume occupied by the electrons increases. This occurs in compounds containing electron-withdrawing groups, which makes the movement of electrons looser, resulting in a high dipole moment value in both compounds **5d** and **6**, this explained the highest activity of both compounds.[76]

Additionally, HOMO and LUMO are crucial properties for figuring out the reactivity of the precursor compound **3**, the essential cyanoacetohydrazide scaffold, and their produced products **4**, **5a–d**, and **6** and they are useful tools for exploring several crucial parameters for calculating a variety of significant parameters like the absolute electronegativity (χ), the chemical potential (P_i), the chemical hardness (η), the chemical softness (S) and the global electrophilicity (ω), these parameters have been under the spotlight for the purpose of interpreting several chemical reactions, as well as structure–activity relationships.[77,78] Table 10 and Fig. 11 showed that the energy difference between HOMO and LUMO (energy gap, ΔE) for compounds **4–6** in the range of 2.7859–3.8746 eV according to the following order of **6** < **4**< **5c** < **5a**< **5b** < **5d** and the hardness values η ranging from 1.3929 for compound **6** to 1.937 for compound **5d**, these values make the electronic transition within these compounds easy depending on the behavior of each moiety. For example, compound **5d** has a relatively higher energy gap (3.8746 eV) than other compounds due to 4-Cl phenyl, which reduces the tendency of HOMO electrons to transfer to LUMO orbitals, whereas

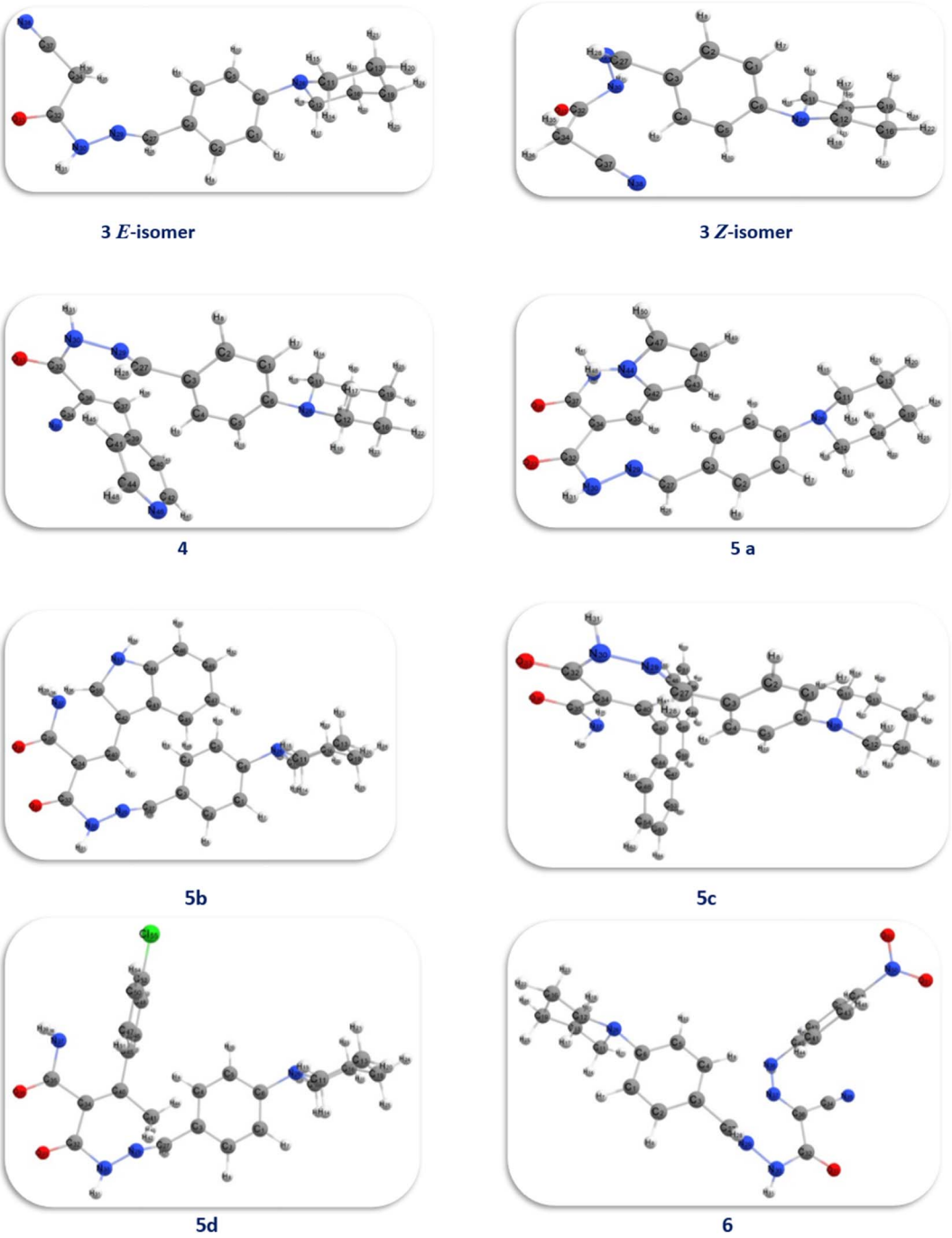

Fig. 10 Optimized model of compounds 3, 4, 5a–d and 6.

compound **6** has the lowest energy gap (ΔE = 2.7859 eV) and the maximum softness (0.7179 eV^{-1}) according to the theoretical calculations, it may illustrated by the presence of CN group and the 4-nitro phenyl ring this two withdrawing group have an excellent inductive properties which polarize the aromatic ring more strongly, making this aromatic-compound less effective against anticancer.[79,80]

Due to the specified electrophilicity and electron flow between donor and acceptor, compounds **4** and **6** exhibited the highest electrophilicity index (ω) values of 5.6125 eV and 9.0650 eV, respectively. In addition, the distribution of atomic charges affects the determination of the electronic chemical vector potential (P_i) in compounds, which is built on the position of negative and positive charges. The (P_i) values of all investigated compounds were between −3.5921 and −5.0253 eV. This high negative chemical potential value means that these compounds are a soft molecule with a high polarizability.[81]

Physicochemical properties of the molecular structure are taught through the MEP. DFT calculation using the optimized

Table 10 Physical descriptors of compounds 3, 4, 5a–d and 6

No.	(E_T) (a.u)	Dipole moment	E_{HOMO} (eV)	E_{LUMO} (eV)	ΔE (eV)	χ (eV)	η (eV)	S (eV)$^{-1}$	P_i (eV)	ω (eV)
3 (*E*)	−876.69	11.6960	−5.7668	−1.8781	3.8887	3.8225	1.9443	0.5143	−3.8225	3.7573
3 (*Z*)	−876.68	8.5526	−5.8926	−1.7151	4.1774	3.8038	2.0887	0.4787	−3.8038	3.4636
4	−1161.87	7.5834	−5.6868	−2.616	3.0707	4.1514	1.5353	0.6512	−4.1514	5.6125
5a	−1200.26	6.2518	−5.5043	−1.9246	3.5796	3.7144	1.7898	0.5587	−3.7144	3.8543
5b	−1353.90	6.2859	−5.4477	−1.7366	3.7110	3.5921	1.8555	0.5389	−3.5921	3.4770
5c	−1529.60	7.2529	−5.4936	−2.2062	3.2874	3.8499	1.6437	0.6083	−3.8499	4.5088
5d	−1721.22	7.6637	−5.6354	−1.7608	3.8746	3.6981	1.9373	0.5161	−3.6981	3.5297
6	−1421.57	8.3540	−6.4183	−3.6324	2.7859	5.0253	1.3929	0.7179	−5.0253	9.0650

structure with the same basis set was used to determine MEP surface analysis of the compound for prediction of relative reactivity positions in a species to resist nucleophilic and electrophilic attacks as shown in Fig. 12. The color code of the compound is between 6.687×10^{-2} (blue region) and -6.687×10^{-2} (red region), these two regions in the MEP structure

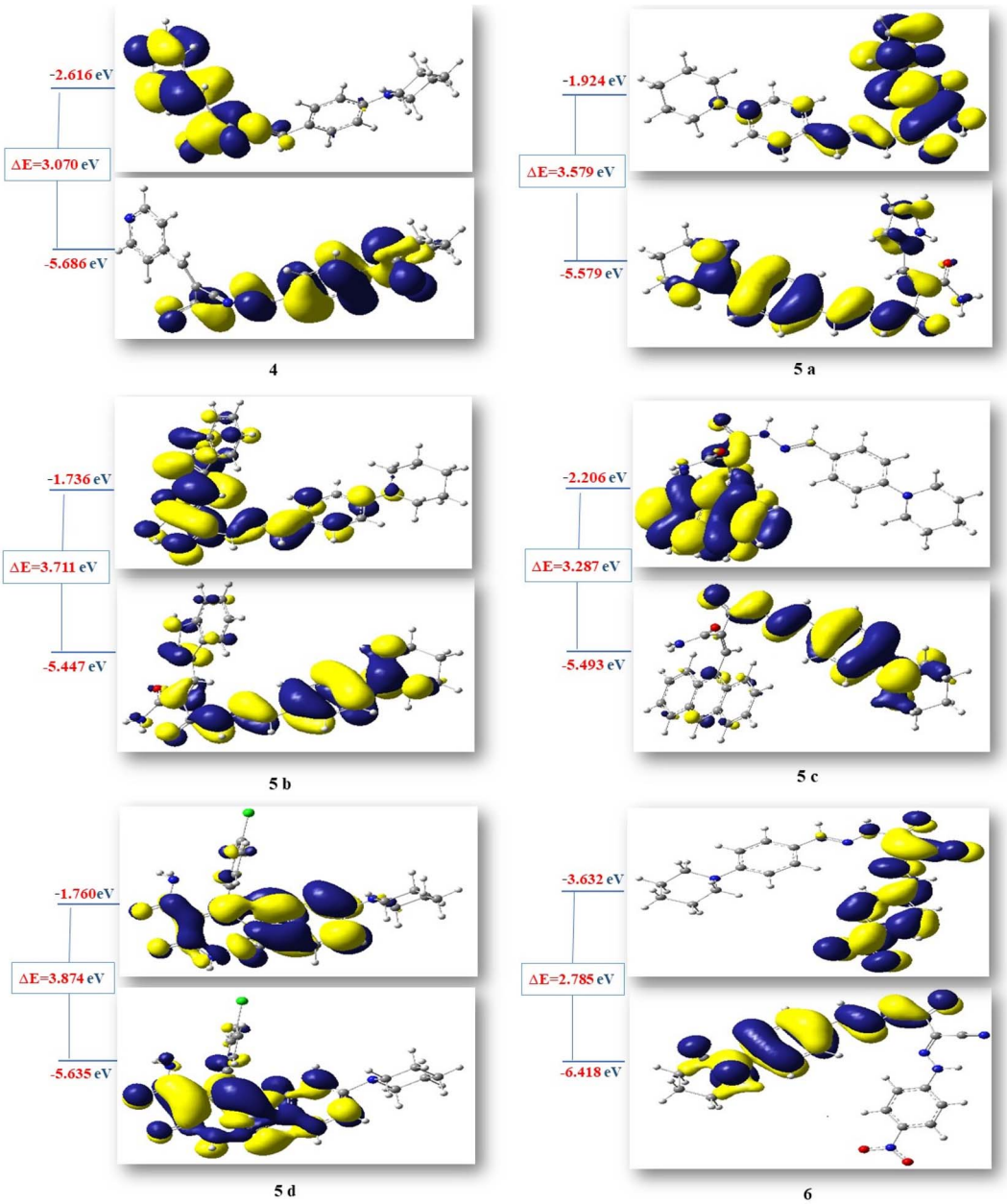

Fig. 11 HOMO–LUMO energy gap (eV) of compounds 4, 5a–d and 6.

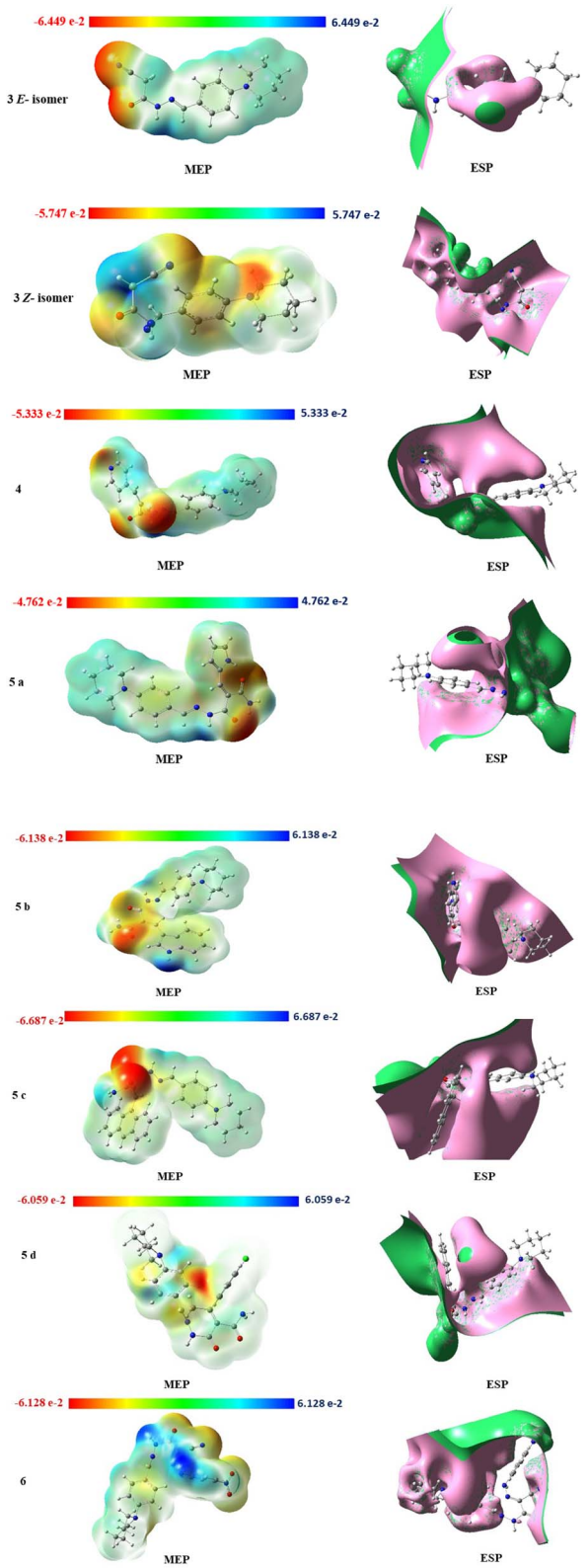

Fig. 12 MEP isosurfaces and ESP isosurfaces of compounds 3, 4, 5a–d and 6.

indicate an electron-rich region, which are localized over the electronegative atoms (oxygen, and nitrogen), and an electron-poor region, respectively.

The electrostatic potential surface ESP (Fig. 12) indicates the distance from the molecule where the (+) charge experiences a predetermined attraction or repulsion that defines the local (−) and (+) potential regions in the molecule to predict the interaction of the charge with both the electron cloud and fixed nuclei. In our investigated compounds, the most of the interaction bonds between compounds **5b**, **5c** and **5d** are due to electron charges of the cyanoacetohydrazide moiety which connected to different aromatic rings.

7 Conclusion

Under Knoevenagel condensation reaction, by using ultrasonic methodology, a series of arylidenes derivatives **4** and **5a–d** was synthesized through reaction of cyanoacetohydrazide derivative **3** with different aldehydes such as isonicotinaldehyde, 1*H*-pyrrole-2-carbaldehyde, 1*H*-indole-3-carbaldehyde and anthracene-9-carbaldehyde, beside 4-chloroacetophenone as a ketone, respectively. Further, reaction of cyanoacetohydrazide derivative **3** with 4-nitrobenzene diazonium chloride gave the hydrazone derivative **6**. All the synthesized compounds were conspicuously interpreted using different spectroscopic analyses such as IR, ^{1}H and ^{13}C NMR and mass spectra. The anti-proliferative screening results of the synthesized compounds against four different human cancer cell lines; hepatocellular carcinoma (HEPG-2), mammary gland breast cancer (MCF-7), colorectal carcinoma colon cancer (HCT-116) and human prostate cancer (PC-3), the majority of tested compounds showed a significant cytotoxic activity towards certain cancer cell and have been targeted for further studies. Gratifyingly, compounds **5d** and **6** showed the highest cytotoxic activity. Meanwhile, compound **5c** proved to have the weakest activity.

Based on the correlation coefficient values, five chemical descriptors were chosen as inputs for creating the QSAR model using the MLR technique: AATS6p, AATS7p, AATS8p, AATS0i, and SpMax4_Bhv. Internal and external validations were used to assess and evaluate the generated QSAR models for statistical significance and predictive capability. The examination of the constructed QSAR model equations revealed that the selected descriptors influence the tested compound's anti-proliferative activity. The descriptors identified in this work by QSAR models can be utilized to predict the anticancer activity levels of novel arylidenes derivatives. This will allow for significant cost savings in the drug development process and synthesis at pharmaceutical chemistry laboratories.

According to the physicochemical properties, all compounds follow Lipinski's Rule of Five and they may exhibit drug-relevant features that should be investigated further in future studies. The results of the probable molecular mechanism for the promising candidate compounds (**5d** and **6**) revealed the presence of adenosine A1 receptor (ADORA1) as a common target for both compounds. ADORA1 receptor activation can be involved in multiple types of cancer cells including colon cancer, breast cancer, leukemia, and melanoma. The docking study of tested compounds **5d** and **6** revealed that their binding scores to the ADORA1 ligand binding site were more favorable as compared to that of its selective antagonist (DU172) and endogenous

Table 11 Summary of ligand binding pocket grid box dimensions

Spacing	n.pts (x; y; z)	Center (x; y; z)
	42; 30; 40	55.151; 58.867; 143.833

agonist (adenosine) suggesting that the anticancer activities of the tested compounds may be related to their ability to block the action of the ADORA1 receptor signaling in cancer cells, leading to cell death. Noteworthy, the computational study *via* DFT and MEP indicated that the theoretical data was found to be in good agreement with the experimental values of compounds *in vitro*.

8. Experimental

8.1. Chemistry

8.1.1. General information. The purity of the synthesized compounds and the progress of all reactions were monitored by thin-layer chromatography (TLC), which was performed on Merck precoated silica gel 60 F254 aluminum sheets, and spots were visualized by a UV lamp at 254 nm. All melting points are uncorrected and were measured using an electric melting point apparatus (G-K). IR spectra (400–4000 cm^{-1}) were performed in KBr disc on the Nicolet iS10 FT-IR spectrometer. ^{1}H NMR (at 400 MHz) and ^{13}C NMR (at 100 MHz) spectra were recorded on a Varian Gemini spectrometer using tetramethylsilane (TMS) as an internal standard in deuterated dimethylsulphoxide (DMSO-d_6). Mass spectra were recorded on a Shimadzu GCMS-QP 1000 EX mass spectrometer at 70 eV at the Regional Center for Mycology and Biotechnology of Al-Azhar University. Elemental analyses were carried out by PerkinElmer 2400 CHN elemental analyzer.

4-(Piperidin-1-yl)benzaldehyde **1** (ref. 42) and cyanoacetohydrazide **2** (ref. 43) were previously prepared according to literature methods.

*2-Cyano-N′-(4-(piperidin-1-yl)benzylidene)acetohydrazide **3***

Method A. A mixture of 4-(piperidin-1-yl)benzaldehyde **1** (1.89 g, 0.01 mol) and cyanoacetohydrazide **2** (0.99 g, 0.01 mol) in ethanol (30 ml) containing drops of AcOH was heated under reflux for 3 h. The solid product which formed on hot was collected by filtration, dried well and then recrystallized from ethanol to afford **3**, yield: 69%.

Method B. A mixture of 4-(piperidin-1-yl)benzaldehyde **1** (1.89 g, 0.01 mol) and cyanoacetohydrazide **2** (0.99 g, 0.01 mol) in ethanol (30 ml) containing drops of AcOH was subjected to ultrasonic energy for 30 min. at 50 °C. The precipitated solid was filtered off, dried well and then recrystallized from ethanol to afford **3**, yield: 90%.

3: as pale-yellow crystals; m.p.: 200–202 °C. IR (KBr, ν/cm^{-1}): 3201 (NH), 2968, 2932, 2832 (C–H_{aliph}), 2263 (C≡N), 1701 (C=O), 1610 (C=N). ^{1}H NMR (400 MHz, DMSO-d_6) δ (ppm): 7.49 (d, 2H, Ar-H, H_o, J = 8.8 Hz), 6.93 (d, 2H, Ar-H, H_m, J = 9.2 Hz), 3.23 (br. s, 4H, N(CH_2)$_2$), 1.57 (br. s, 6H, CH_2–(CH_2)$_3$–CH_2), for *E*-isomer [11.53 (s, 1H, NH, exchangeable with D_2O), 7.86 (s, 1H, CH=N), 4.13 (s, 2H, CH_2CN), for *Z*-isomer [11.43 (s, 1H, NH, exchangeable with D_2O), 8.00 (s, 1H, (HC=N), 3.74 (s, 2H, CH_2CN)]. ^{13}C NMR (100 MHz, DMSO-d_6) δ (ppm): 164.1, 158.2, 152.5, 152.4, 148.1, 144.8, 128.5, 128.2, 122.8, 122.6, 116.1, 115.8, 114.5, 114.4, 48.3 (2), 24.9 (2), 24.2, 23.9. MS *m*/*z* (%): 270.58 ($M^{\bullet+}$; 62.95). Anal. Calcd. for $C_{15}H_{18}N_4O$ (270.34): C, 66.64; H, 6.71; N, 20.73. Found: C, 66.59; H, 6.68; N, 20.83.

*General method for synthesis of arylidene derivatives **4** and **5a–d**.* A mixture of compound **3** (2.7 g, 0.01 mol) and appropriate aldehydes and/or ketone, namely isonicotinaldehyde, 1*H*-pyrrole-2-carbaldehyde, 1*H*-indole-3-carbaldehyde, anthracene-9-carbaldehyde, and 4-chloroacetophenone (0.01 mol), in ethanol (30 ml) containing a few drops of piperidine was sonicated for 2 h (for isonicotinaldehyde) and/or 4 h (for the others) at 75 °C. After cooling the resulting mixture at ambient temperature was poured into ice/water and acidified with dilute acetic acid. The precipitated solid was filtered off, washed several times with cold water, dried well and then recrystallized from the appropriate solvent to afford the arylidene derivatives **4** and **5a–d**.

*2-Cyano-N′-(4-(piperidin-1-yl)benzylidene)-3-(pyridin-4-yl) acrylohydrazide **4**.* As dark yellow crystals (ethanol); m.p.: 280–282 °C, yield: 80%. IR (KBr, ν/cm^{-1}): 3283 (NH), 2938, 2851 (C-H_{aliph}), 2200 (C≡N), 1682 (C=O), 1604 (C=N or C=C). ^{1}H NMR (400 MHz, DMSO-d_6) δ (ppm): 11.35 (s, 1H, NH, exchangeable with D_2O), 8.28 (s, 1H, HC=N), 8.01 (s, 1H, HC=C), 7.91 (br. s, 2H, $C_{2,6}$–$H_{(pyridine)}$), 7.53 (d, 2H, Ar-H, H_o, J = 8.0 Hz), 7.04 (d, 2H, $C_{3,5}$–$H_{(pyridine)}$, J = 8.8 Hz), 6.96 (d, 2H, Ar-H, H_m, J = 8.0 Hz), 3.46 (t, 4H, *N*-(CH_2)$_2$, J = 5.2 Hz, J = 4.8 Hz), 1.58 (br.s, 6H, –CH_2–(CH_2)$_3$–CH_2–). ^{13}C NMR (100 MHz, DMSO-d_6) δ (ppm): 167.4, 152.8, 150.2, 148.3 (2), 140.5, 137.8, 132.1, 132.0 (2), 129.1 (2), 115.0 (2), 113.8, 112.3, 48.8 (2), 30.2 (2), 28.8. MS *m*/*z* (%): 359.21 ($M^{\bullet+}$; 35.57). Anal. Calcd. for $C_{21}H_{21}N_5O$ (359.43): C, 70.17; H, 5.89; N, 19.48. Found: C, 70.20; H, 5.97; N, 19.44.

*2-(2-(4-(Piperidin-1-yl)benzylidene)hydrazine-1-carbonyl)-3-(1H-pyrrol-2-yl)acrylamide **5a**.* As brown crystals (water); m.p.: 258–260 °C, yield: 92%. IR (KBr, ν/cm^{-1}): 3355, 3220, 3190 (NH_2, NH), 2928, 2850 (C-H_{aliph}), 1684, 1663 (C=O), 1598 (C=C). ^{1}H NMR (400 MHz, DMSO-d_6) δ (ppm): 14.1 (s, 1H, NH, exchangeable with D_2O), 10.47 (s, 1H, NH, exchangeable with D_2O), 9.68 (s, 1H, HC=N), 7.68 (d, 2H, Ar-H, H_o, J = 8.8 Hz), 7.63 (s, 1H, HC=C), 7.47 (br. s, 1H, C_5–$H_{pyrrole}$), 7.01 (d, 2H, Ar-H, H_m, J = 8.8 Hz), 6.86 (t, 1H, C_4–$H_{pyrrole}$), 6.41 (br. s, 1H, C_3-$H_{pyrrole}$), 5.69 (br. s, 2H, NH_2, exchangeable with D_2O), 3.42 (t, 4H, *N*-(CH_2)$_2$, J = 5.6 Hz, J = 4.4 Hz), 1.59–1.57 (m, 6H, –CH_2–(CH_2)$_3$–CH_2–). ^{13}C NMR (100 MHz, DMSO-d_6) δ (ppm): 165.1, 164.9, 154.8, 153.3, 131.9, 129.6, 129.4, 128.5, 128.3, 125.5, 123.0, 113.2 (2), 112.7, 112.0, 47.8 (2), 25.0 (2), 24.1. MS *m*/*z* (%): 347.38 ($M^{\bullet+}$–H_2O; 35.89). Anal. Calcd. for $C_{20}H_{23}N_5O_2$ (365.44): C, 65.73; H, 6.34; N, 19.16. Found: C, 65.74; H, 6.31; N, 19.18.

*3-(1H-Indol-3-yl)-2-(2-(4-(piperidin-1-yl)benzylidene)hydrazine-1-carbonyl)acrylamide **5b**.* As dark red crystals (ethanol); m.p.: 123–125 °C, yield: 72%. IR (KBr, ν/cm^{-1}): 3367, 3320, 3216 (NH_2, NH), 2932, 2852 (C-H_{aliph}), 1650 (C=O), 1594 (C=C). ^{1}H NMR (400 MHz, DMSO-d_6) δ (ppm): 12.06 (br. s, 2H, 2NH, exchangeable with D_2O), 9.93 (s, 1H, HC=N), 9.67 (s, 1H, HC=C), 8.27 (s, 1H, C_2–$H_{(indole)}$), 8.09 (d, 1H, C_4–$H_{(indole)}$, J = 7.2 Hz),

7.67 (d, 2H, Ar-H, H_o, $J = 8.8$ Hz), 7.51 (d, 1H, C_7–$H_{(indole)}$, $J = 7.6$ Hz), 7.27–7.19 (m, 2H, $2C_{5,6}$–$H_{(indole)}$), 7.00 (d, 2H, Ar-H, H_m, $J = 8.8$ Hz), 3.40 (br. s, 4H, *N*-$(CH_2)_2$), 3.10 (br. s, 2H, NH_2, exchangeable with D_2O), 1.58 (br. s, 6H, –CH_2–$(CH_2)_3$–CH_2–). ^{13}C NMR (100 MHz, DMSO-d_6) δ (ppm): 189.9, 184.9, 154.6 (2), 138.4, 137.0, 131.6 (2), 125.4 (2), 124.1, 123.4, 122.0, 120.8, 118.1, 113.8, 113.0 (2), 112.4, 47.6 (2), 23.9 (2), 22.2. MS *m*/*z* (%): 415.97 ($M^{\bullet+}$; 36.71). Anal. Calcd. for $C_{24}H_{25}N_5O_2$ (415.50): C, 69.38; H, 6.07; N, 16.86. Found: C, 69.42; H, 6.20; N, 16.83.

3-(Anthracen-9-yl)-2-(2-(4-(piperidin-1-yl)benzylidene)hydrazine-1-carbonyl)acrylamide ***5c***. As red crystals (ethanol/water); m.p.: 122–124 °C, yield: 53%. IR (KBr, ν/cm^{-1}): 3453, 3338, 3229 (NH_2, NH), 2953, 2874, 2809 (C–H_{aliph}), 1658 (C=O), 1623 (C=N or C=C). ^{1}H NMR (400 MHz, DMSO-d_6) δ (ppm): 10.50 (br. s, 1H, NH, exchangeable with D_2O), 9.04 (d, 2H, Ar-H, $J = 9.6$ Hz), 9.02 (s, 1H, HC=N), 8.78 (s, 1H, C_{10}–$H_{anthracene}$), 8.4 (s, 1H, HC=C), 7.96 (d, 2H, $C_{1,8}$–$H_{anthracene}$, $J = 9.2$ Hz), 7.76 (d, 2H, Ar-H, $J = 8$ Hz), 7.75–7.59 (m, 6H, Ar-H), 4.27 (s, 2H, NH_2, exchangeable with D_2O), 3.35 (br. s, 4H, *N*-$(CH_2)_2$), 1.58 (br. s, 6H, –CH_2–$(CH_2)_3$–CH_2–). ^{13}C NMR (100 MHz, DMSO-d_6) δ (ppm): 189.9, 162.5, 154.6, 150.9, 149.2, 138.5, 135.2 (2), 131.6, 131.3 (2), 130.6 (2), 129.3 (2), 128.7, 126.3, 125.8 (2), 125.4, 124.4, 123.4 (2), 113.0 (2), 48.2 (2), 24.8 (2), 23.9. MS *m*/*z* (%): 477.15 ($M^{\bullet+}$ + 1; 34.19), 476.20 ($M^{\bullet+}$; 5.19). Anal. Calcd. for $C_{30}H_{28}N_4O_2$ (476.58): C, 75.61; H, 5.92; N, 11.76. Found: C, 75.59; H, 5.93; N, 11.80.

3-(4-Chlorophenyl)-2-(2-(4-(piperidin-1-yl)benzylidene) hydrazine-1-carbonyl)but-2-enamide ***5d***. As brown crystals (ethanol/water); m.p.: 285–287 °C, yield: 66%. IR (KBr, ν/cm^{-1}): 3196, 3163 (br.) (NH, NH_2), 2933, 2854 (C–H_{aliph}), 1686 (C=O), 1592 (C=C). ^{1}H NMR (400 MHz, DMSO-d_6) δ (ppm): 12.13 (br. s, 1H, NH, exchangeable with D_2O), 10.86 (br. s, 2H, NH_2, exchangeable with D_2O), 8.21 (d, 2H, Ar-H, $J = 8.4$ Hz), 7.77 (d, 2H, Ar-H, $J = 8.4$ Hz), 7.57 (s, 1H, HC=N), 7.56 (d, 2H, Ar-H, $J = 7.2$ Hz), 7.02 (d, 2H, Ar-H, $J = 8.4$ Hz), 3.28 (br.s, 4H, *N*-$(CH_2)_2$), 2.57 (s, 3H, CH_3), 1.61 (br. s, 6H, –CH_2–$(CH_2)_3$–CH_2–). MS *m*/*z* (%): 424.11 ($M^{\bullet+}$; 27.44). ^{13}C NMR (100 MHz, DMSO-d_6) δ (ppm): 189.9, 159.9, 154.6, 151.7, 144.5, 137.8, 134.0, 131.6 (2), 129.5 (2), 128.7 (2), 125.4, 114.1, 113.0 (2), 47.6 (2), 24.8 (2), 23.9, 22.2. Anal. Calcd. for $C_{23}H_{25}ClN_4O_2$ (424.93): C, 65.01; H, 5.93; N, 13.19. Found: C, 65.11; H, 5.94; N, 13.27.

N-(4-Nitrophenyl)-2-oxo-2-(2-(4-(piperidin-1-yl)benzylidene) hydrazinyl)acetohydrazonoyl cyanide ***6***. To *p*-nitroaniline (1.38 g, 0.01 mol) concentrated HCl (3 ml) was added and cooled to 0–5 °C in ice bath then cooled sodium nitrite solution (1.0 g in 10 ml water) was added dropwise to the acidic solution of *p*-nitroaniline. The reaction mixture was then stirred for 10 min to form the diazotized salt of *p*-nitroaniline. To a cold mixture of compound **3** (2.7 g, 0.01 mol) and sodium acetate (4.10 g, 0.05 mol) in ethanol (50 ml), the prepared diazotized salt of *p*-nitroaniline was added dropwise with stirring. The mixture was ultrasonicated at ambient temperature for 30 min. The reaction mixture was left overnight. The precipitated solid was filtered off, dried well and then recrystallized from ethanol to give **6** as black crystals; m.p.: 128–130 °C, yield: 56.5%. IR (KBr, ν/cm^{-1}): 3419, 3195 (NH), 2928, 2855 (C–H_{aliph}), 2215 (C≡N), 1680 (C=O), 1642 (C=N), 1596 (C=C), 1515, 1338 (NO_2). ^{1}H NMR (400 MHz, DMSO-d_6) δ (ppm): 9.66 (br. s, 1H, NH, exchangeable with D_2O), 8.41 (s, 1H, HC=N), 8.32–6.98 (m, 8H, Ar-H), 6.58 (br. s, H, NH, exchangeable with D_2O), 3.38 (br.s, 4H, *N*-$(CH_2)_2$), 1.59 (br. s, 6H, –CH_2–$(CH_2)_3$–CH_2–). ^{13}C NMR (100 MHz, DMSO-d_6) δ (ppm): 155.7, 153.5, 147.7, 142.6, 133.6, 126.4 (2), 125.2 (2), 119.2, 115.9 (2), 112.4 (2), 111.8, 110.8, 47.7 (2), 24.8 (2), 23.9. MS *m*/*z* (%): 419.18 ($M^{\bullet+}$; 21.64). Anal. Calcd. for $C_{21}H_{21}N_7O_3$ (419.45): C, 60.13; H, 5.05; N, 23.38. Found: C, 60.07; H, 5.24; N, 23.22.

8.2. Cytotoxicity and antitumor evaluation

Antitumor activity was tested at the drugs department, Faculty of Pharmacy, Mansoura University, Egypt.

8.2.1. Materials and methods

8.2.1.1 Cell line. Four human tumor cell lines namely, hepatocellular carcinoma (HEPG-2), mammary gland breast cancer (MCF-7), colorectal carcinoma colon cancer (HCT-116) and human prostate cancer (PC-3). The cell lines were obtained from ATCC *via* Holding company for biological products and vaccines (VACSERA), Cairo, Egypt. For comparison, doxorubicin was utilized as a standard anticancer drug.

8.2.2. MTT assay. The MTT assay was performed to evaluate the synthesized compounds' inhibitory effects on cell proliferation against the aforementioned cell lines.[82,83] The ability of mitochondrial succinate dehydrogenase in live cells to convert yellow tetrazolium bromide (MTT) (Sigma Co., St. Louis, USA) into a purple formazan derivative is used in this colorimetric experiment. Cell lines were cultured in RPMI-1640 media supplemented with 10% foetal bovine serum (GIBCO, UK) (Sigma Co., St. Louis, USA). Sigma Co., St. Louis, USA) antibiotics in the concentrations of 100 units per ml penicillin and 100 g ml^{-1} streptomycin were added (Shedon. TC2323. Cornelius, OR, USA).

The cell lines were seeded in a 96-well plate at a density of 10^4 cells per well and incubated at 37 °C for 48 hours with 5% CO_2. The cells were cultured for 24 hours after being exposed to various chemical concentrations. After a 24-hours incubation period, 20 μl of a 5 mg ml^{-1} MTT solution was added and incubated for 4 hours. To dissolve the generated purple formazan, each well receives 100 μl of dimethyl sulfoxide (DMSO) (Sigma Co., St. Louis, USA). The colorimetric assay is measured and recorded at wavelength of 570 nm using a plate reader (EXL 800, USA). The proportion of relative cell viability was estimated as (A_{570} of treated samples/A_{570} of untreated sample) × 100.

8.3. Docking studies

AutoDock Vina modeling simulation software (AutoDock Vina v.1.2.0) was used to predict the protein-ligand binding affinity, as well as the preferred orientation of the docking pose between the amino acid residues that form the ligand binding pocket of the ADORA1 receptor and the studied compounds **5d** and **6**, in addition to the receptor endogenous agonist (adenosine) and DU172 (selective ADORA1 antagonists) that were used as reference ligand. The 3D-structure of ADORA1 protein bound to the co-crystalized ligand, DU172, was downloaded from Protein Data Bank (PDB) (**https://www.rcsb.org**) at a resolution of 3.2 (PDB: 5uen).

PyMOL molecular visualization tool (PyMOL v.2.5.4) (Schrödinger, Inc.) was used to extract the ADORA1 receptor from its

co-crystalized DU172, after adding hydrogen bonds to both. The extracted files were in PDB format.[84] Auto-Dock (MGL-tools) was used to determine the docking site and the grid box dimensions of ligand binding pocket.[85] The grid box dimensions were selected by centering grid box on the Du172 ligand, included in crystal structure (Table 11). Moreover, the target protein and the tested compounds were exported in PDBQT format (AutoDock format) using Open Babel v.2.3.1.[86]

A maximum of 9 poses was considered for each molecule where the target protein was kept as the rigid receptor while keeping the conformation of the ligands as flexible.[87] Finally, the most favorable pose was selected according to the minimum free energy of the protein–ligand complex and for analyzing the type of interactions between the ligand and the protein, BIOVIA Discovery Studio (DS) Visualizer v.4.5. was used.

8.4. DFT theoretical calculations

The investigated compounds were theoretically calculated using Gaussian 09 software (2009, Gaussian 09, Revision A.1, Gaussian. Inc.: Wallingford, CT, USA).[88] The DFT computations were carried out using the B3LYP 6-31G (d,p) basis set. The structural geometry was strengthened by evading the molecular symmetry restrictions in contrast to all geometrical variables and by minimizing its energy. The optimized compounds' molecular structure was sketched using Gauss View.[89]

Conflicts of interest

There are no conflicts to declare.

References

1 E. Nassar, Y. A.-M. El-Badry and H. El Kazaz, *Chem. Pharm. Bull.*, 2016, **64**, 558–563.
2 A. M. Fahim, H. S. Magar, E. Nasar, F. M. Abdelrazek and A. Aboelnaga, *J. Inorg. Organomet. Polym. Mater.*, 2022, **32**, 240–266.
3 M. M. Abdelshaheed, I. M. Fawzy, H. I. El-Subbagh and K. M. Youssef, *Future Journal of Pharmaceutical Sciences*, 2021, **7**, 1–11.
4 P. Goel, O. Alam, M. J. Naim, F. Nawaz, M. Iqbal and M. I. Alam, *Eur. J. Med. Chem.*, 2018, **157**, 480–502.
5 S. N. Mokale, P. N. Dube, S. A. Bhavale, I. Sayed, A. Begum, M. C. Nevase, V. R. Shelke and A. Mujaheed, *Med. Chem. Res.*, 2015, **24**, 1842–1856.
6 A. Aboelnaga, E. Mansour, A. M. Fahim and G. H. Elsayed, *J. Mol. Struct.*, 2022, **1251**, 131945.
7 R. N. Asha, M. Sankarganesh, N. Bhuvanesh and B. R. D. Nayagam, *J. Mol. Struct.*, 2022, **1250**, 131692.
8 Z.-S. Gu, W.-T. Wang, H. Qian, A.-N. Zhou, H.-B. Sun, Q.-W. Zhang and J.-Q. Li, *Bioorg. Med. Chem. Lett.*, 2019, **29**, 126703.
9 F. Xiao, R. Yan, Y. Zhang, S. Wang, S. Chen, N. Zhou and X. Deng, *Arch. Pharm.*, 2021, **354**, 2000298.
10 J. Jayabharathi, A. Manimekalai, T. C. Vani and M. Padmavathy, *Eur. J. Med. Chem.*, 2007, **42**, 593–605.
11 G. Aridoss, S. Balasubramanian, P. Parthiban and S. Kabilan, *Eur. J. Med. Chem.*, 2007, **42**, 851–860.
12 M. G. Abouelenein, A. E.-H. A. Ismail, A. Aboelnaga, M. A. Tantawy, N. M. El-Ebiary and S. A. El-Assaly, *J. Mol. Struct.*, 2023, **1275**, 134587.
13 S. Wang, A. Haikarainen, A. Pohjakallio, J. Sipilä, J. Kaskinoro, S. Juhila, N. Jalava, M. Koskinen, M. Vesajoki and E. Kumpulainen, *Bioorg. Med. Chem. Lett.*, 2022, **69**, 128783.
14 S. McElvain and T. P. Carney, *J. Am. Chem. Soc.*, 1946, **68**, 2592–2600.
15 S. A. Khanum, V. Girish, S. Suparshwa and N. F. Khanum, *Bioorg. Med. Chem. Lett.*, 2009, **19**, 1887–1891.
16 M. N. Yousif, *Mini-Rev. Org. Chem.*, 2022, **19**, 125–135.
17 S. Sivakumar, *Chem. Sci. Rev. Lett.*, 2016, **5**, 99–105.
18 M. SV, S. Belagali and M. Bhat, *Anti-Infect. Agents*, 2020, **18**, 362–374.
19 S. Deekonda, J. Cole, S. Sunna, D. Rankin, T. M. Largent-Milnes, P. Davis, N. M. BassiriRad, J. Lai, T. W. Vanderah and F. Porecca, *Bioorg. Med. Chem. Lett.*, 2016, **26**, 222–227.
20 E. Vitaku, D. T. Smith and J. T. Njardarson, *J. Med. Chem.*, 2014, **57**, 10257–10274.
21 M. R. Mahmoud, S. A. Shiba, A. K. El-Ziaty, F. S. M. Abu El-Azm and M. F. Ismail, *Synth. Commun.*, 2014, **44**, 1094–1102.
22 M. F. Ismail and A. A. El-sayed, *J. Iran. Chem. Soc.*, 2018, **16**, 921–937.
23 S. A. Shaker and M. I. Marzouk, *Molecules*, 2016, **21**, 155.
24 M. F. Ismail and G. A. Elsayed, *Synth. Commun.*, 2018, **48**, 892–905.
25 M. R. Mahmoud, A. K. El-Ziaty, F. S. A. El-Azm, M. F. Ismail and S. A. Shiba, *J. Chem. Res.*, 2013, **37**, 80–85.
26 M. F. Ismail, A. F. Aly, S. S. Abdel-Wahab and A. A. El-Sayed, *Polycyclic Aromat. Compd.*, 2023, **43**, 1288–1308.
27 N. A. Hamed, M. I. Marzouk, M. F. Ismail and M. H. Hekal, *Synth. Commun.*, 2019, **49**, 3017–3029.
28 M. H. Hekal, Y. M. Ali and F. S. M. Abu El-Azm, *Synth. Commun.*, 2020, **50**, 2839–2852.
29 M. A. Gouda, M. A. Salem, M. I. Marzouk, N. F. Mahmoud and M. F. Ismail, *Chem. Biodiversity*, 2023, **20**, e202300706.
30 H. M. Refat and A. A. Fadda, *Eur. J. Med. Chem.*, 2013, **70**, 419–426.
31 H. Hosseini and M. Bayat, *Top. Curr. Chem.*, 2018, **376**, 40.
32 D. Priya, P. Gopinath, L. S. Dhivya, A. Vijaybabu, M. Haritha, S. Palaniappan and M. K. Kathiravan, *ChemistrySelect*, 2022, **7**, e202104429.
33 M. R. Mahmoud, F. S. M. Abu El-Azm, A. T. Ali and Y. M. Ali, *Synth. Commun.*, 2017, **47**, 1591–1600.
34 M. A. Salem, S. Y. Abbas, M. H. Helal and A. Y. Alzahrani, *J. Heterocycl. Chem.*, 2021, **58**, 2117–2123.
35 A. M. M. Mohamed, M. F. Ismail, H. M. F. Madkour, A. F. Aly and M. S. Salem, *Synth. Commun.*, 2020, **50**, 3424–3442.
36 M. F. Ismail, A. I. Hashem, R. A. Sleem and A. I. Hassaballah, *ChemistrySelect*, 2023, **8**, e202204946.
37 A. N. El-hoshoudy, M. A. El-Raouf, M. M. Attya, A. F. Ahmed and M. Waly, *J. Chem. Appl.*, 2021, 33–53, DOI: **10.36811/jca.2021.110009**.

38 A. Aboelnaga, M. Hagar and S. M. Soliman, *Molecules*, 2016, **21**, 848.
39 C. Hazra, S. Tonde, B. Dhanvijay, D. Kundu, A. Satdive, S. Tayde, B. Toksha, J. Naik and A. Chatterjee, *Chem. Eng. J.*, 2023, **451**, 138996.
40 S. Soror, A. M. Fahim, S. Elabbady, E. Nassar and A. Aboelnaga, *J. Biomol. Struct. Dyn.*, 2022, **40**, 5409–5426.
41 A. M. Fahim, E. H. I. Ismael, G. H. Elsayed and A. M. Farag, *J. Biomol. Struct. Dyn.*, 2022, **40**, 9177–9193.
42 M. S. A. El-Gaby, *J. Chin. Chem. Soc.*, 2004, **51**, 125–134.
43 S. H. Doss, W. W. Wardakhan and N. A. Louca, *Arch. Pharmacal Res.*, 2001, **24**, 377–384.
44 G. Minotti, P. Menna, E. Salvatorelli, G. Cairo and L. Gianni, *Pharmacol. Rev.*, 2004, **56**, 185–229.
45 C. Y. Hong, Y. K. Kim, J. H. Chang, S. H. Kim, H. Choi, D. H. Nam, Y. Z. Kim and J. H. Kwak, *J. Med. Chem.*, 1997, **40**, 3584–3593.
46 S. Şenkardeş, M. İ. Han, N. Kulabaş, M. Abbak, Ö. Çevik, İ. Küçükgüzel and Ş. G. Küçükgüzel, *Mol. Diversity*, 2020, **24**, 673–689.
47 N. Hristova-Avakumova, K. Yoncheva, B. Nikolova-Mladenova, T. Traykov, G. Momekov and V. Hadjimitova, *Redox Rep.*, 2017, **22**, 408–417.
48 S. Benaka Prasad, K. Vinaya, C. Ananda Kumar, S. Swarup and K. Rangappa, *Med. Chem. Res.*, 2010, **19**, 220–235.
49 S. Vilar, G. Cozza and S. Moro, *Curr. Top. Med. Chem.*, 2008, **8**, 1555–1572.
50 S. Chtita, M. Ghamali, A. Ousaa, A. Aouidate, A. Belhassan, A. I. Taourati, V. H. Masand, M. Bouachrine and T. Lakhlifi, *Heliyon*, 2019, **5**, 1–26.
51 A. Tropsha, *Mol. Inf.*, 2010, **29**, 476–488.
52 K. Roy, S. Kar and R. N. Das, *Understanding the Basics of QSAR for Applications in Pharmaceutical Sciences and Risk Assessment*, Academic press, 2015.
53 C. W. Yap, *J. Comput. Chem.*, 2011, **32**, 1466–1474.
54 T. Lumley and A. Miller, *_leaps: Regression Subset Selection_. R package version 3.1*, 2020, Retrieved from **https://CRAN.R-project.org/package=leaps**.
55 R. Kiralj and M. Ferreira, *J. Braz. Chem. Soc.*, 2009, **20**, 770–787.
56 D. E. Arthur, A. Uzairu, P. Mamza, S. E. Abechi and G. Shallangwa, *J. King Saud Univ., Sci.*, 2020, **32**, 324–331.
57 S. N. Adawara, G. A. Shallangwa, P. A. Mamza and A. Ibrahim, *Beni-Suef University Journal of Basic and Applied Sciences*, 2020, **9**, 1–17.
58 A. Lagunin, A. Zakharov, D. Filimonov and V. Poroikov, *Mol. Inf.*, 2011, **30**, 241–250.
59 R. W. Kennard and L. A. Stone, *Technometrics*, 1969, **11**, 137–148.
60 V. Catalani, M. Botha, J. M. Corkery, A. Guirguis, A. Vento, N. Scherbaum and F. Schifano, *Pharmaceuticals*, 2021, **14**, 720.
61 Y. Isyaku, A. Uzairu, S. Uba, M. T. Ibrahim and A. B. Umar, *Bulletin of the National Research Centre*, 2020, **44**, 1–11.
62 S. Chtita, A. Belhassan, M. Bakhouch, A. I. Taourati, A. Aouidate, S. Belaidi, M. Moutaabbid, S. Belaaouad, M. Bouachrine and T. Lakhlifi, *Chemom. Intell. Lab. Syst.*, 2021, **210**, 104266.
63 C. A. Lipinski, F. Lombardo, B. W. Dominy and P. J. Feeney, *Adv. Drug Delivery Rev.*, 2012, **64**, 4–17.
64 G. R. Bickerton, G. V. Paolini, J. Besnard, S. Muresan and A. L. Hopkins, *Nat. Chem.*, 2012, **4**, 90–98.
65 A. Daina, O. Michielin and V. Zoete, *Nucleic Acids Res.*, 2019, **47**, W357–W364.
66 A. Townsend-Nicholson, P. Schofield and E. Baker, *Genomics*, 1995, **26**, 423–425.
67 B. B. Fredholm, A. P. IJzerman, K. A. Jacobson, K.-N. Klotz and J. Linden, *Pharmacol. Rev.*, 2001, **53**, 527–552.
68 H.-E. Khoo, C.-L. Ho, V. J. Chhatwal, S. T. Chan, S.-S. Ngoi and S. M. Moochhala, *Cancer Lett.*, 1996, **106**, 17–21.
69 A. Mirza, A. Basso, S. Black, M. Malkowski, L. Kwee, J. A. Patcher, J. E. Lachowicz, Y. Wang and S. Liu, *Cancer Biol. Ther.*, 2005, **4**, 1355–1360.
70 S. Gessi, K. Varani, S. Merighi, A. Morelli, D. Ferrari, E. Leung, P. G. Baraldi, G. Spalluto and P. A. Borea, *Br. J. Pharmacol.*, 2001, **134**, 116–126.
71 S. Merighi, K. Varani, S. Gessi, E. Cattabriga, V. Iannotta, C. Ulouglu, E. Leung and P. A. Borea, *Br. J. Pharmacol.*, 2001, **134**, 1215–1226.
72 S. Ni, Q. Wei and L. Yang, *OncoTargets Ther.*, 2020, **13**, 12409–12419.
73 Z. Lin, P. Yin, S. Reierstad, M. O'Halloran, J. V. Coon, E. Pearson, G. Mutlu and S. Bulun, *Oncogene*, 2010, **29**, 1114–1122.
74 D. S. Shin, K. S. Min and B. G. Kim, *World J. Adv. Res. Rev.*, 2018, **6**, 262712.
75 S. Biswal, U. Sahoo, S. Sethy, H. Kumar and M. Banerjee, *Asian J. Pharm. Clin. Res.*, 2012, **5**, 1–6.
76 J. Rahman, A. M. Tareq, M. M. Hossain, S. A. Sakib, M. N. Islam, M. H. Ali, A. N. Uddin, M. Hoque, M. S. Nasrin and T. B. Emran, *Pharmaceuticals*, 2020, **13**, 232.
77 A. A. El-Sayed, G. A. Elsayed, S. A. Rizk and M. F. Ismail, *Org. Prep. Proced. Int.*, 2023, **16**, 1–14.
78 A. A. El-Sayed, M. F. Ismail, A. E.-G. E. Amr and A. M. Naglah, *Molecules*, 2019, **24**, 3787.
79 H. E. Tolan, A. M. Fahim and E. H. Ismael, *J. Mol. Struct.*, 2023, **1283**, 135238.
80 A. Attia, A. Aboelnaga and A. M. Fahim, *Egypt. J. Chem.*, 2023, **66**, 95–111.
81 M. A. Mumit, T. K. Pal, M. A. Alam, M. A.-A.-A.-A. Islam, S. Paul and M. C. Sheikh, *J. Mol. Struct.*, 2020, **1220**, 128715.
82 T. Mosmann, *J. Immunol. Methods*, 1983, **65**, 55–63.
83 F. Denizot and R. Lang, *J. Immunol. Methods*, 1986, **89**, 271–277.
84 L. Schrödinger and W. DeLano, *PyMOL*, 2020, **http://www.pymol.org/pymol**.
85 G. M. Morris, R. Huey, W. Lindstrom, M. F. Sanner, R. K. Belew, D. S. Goodsell and A. J. Olson, *J. Comput. Chem.*, 2009, **30**, 2785–2791.
86 N. O'Boyle, *J. Cheminf.*, 2011, **3**, 33.
87 J. Eberhardt, D. Santos-Martins, A. F. Tillack and S. Forli, *J. Chem. Inf. Model.*, 2021, **61**, 3891–3898.
88 R. A. Gaussian09, Inc., Wallingford CT, 2009, vol. 121, 150–166.
89 R. Dennington, T. Keith, J. Millam and V. GaussView, *GaussView, Version*, Shawnee Mission KS, 2009, vol. 5.